arXiv:1104.2513v2 [astro-ph.GA] 3 Dec 2011

The Case for the Dual Halo of the Milky Way

Timothy C. Beers[1,2], Daniela Carollo[3,4], Željko Ivezić[5], Deokkeun An[6], Masashi Chiba[7], John E. Norris[3], Ken C. Freeman[3], Young Sun Lee[1], Jeffrey A. Munn[8], Paola Re Fiorentin[9], Thirupathi Sivarani[10], Ronald Wilhelm[11], Brian Yanny[12], Donald G. York[13]

ABSTRACT

Carollo et al. have recently resolved the stellar population of the Milky Way halo into at least two distinct components, an inner halo and an outer halo. This result has been criticized by Schönrich et al., who claim that the retrograde signature associated with the outer halo is due to the adoption of faulty distances. We refute this claim, and demonstrate that the Schönrich et al. photometric distances are themselves flawed because *they adopted an incorrect main-sequence absolute magnitude relationship from the work of Ivezić et al.*. When compared to the recommended relation from Ivezić et al., which is tied to a Milky Way globular cluster distance scale and accounts for age and metallicity effects, the relation adopted by Schönrich et al. yields up to 18% shorter distances for stars near the main-sequence turnoff (TO). Use of the correct relationship yields agreement between the distances assigned by Carollo et al. and Ivezić et al. for low-metallicity dwarfs to within 6-10%. Schönrich et al. also point out that intermediate-gravity stars ($3.5 \leq \log g < 4.0$) with colors redder than the TO region are likely misclassified, with which we concur. We implement a new procedure to reassign luminosity classifications for the TO stars that require it. New derivations of the rotational behavior demonstrate that the retrograde signature and high velocity dispersion of the outer-halo population remains. We summarize additional lines of evidence for a dual halo, including a test of the retrograde signature based on proper motions alone, and conclude that the preponderance of evidence strongly rejects the single-halo interpretation.

[1]Department of Physics & Astronomy and JINA (Joint Institute for Nuclear Astrophysics), Michigan State University, East Lansing, MI 48824, USA; beers@pa.msu.edu; lee@pa.msu.edu

[2]National Optical Astronomical Observatory, Tucson, AZ 85719, USA

[3]Research School of Astronomy & Astrophysics, Australian National University, Mount Stromlo Observatory, Cotter Road, Weston, ACT, 2611, Australia; carollo@mso.anu.edu.au, jen@mso.anu.edu.au; kcf@mso.anu.edu.au

[4]Department of Physics & Astronomy, Macquarie University, Sydney, NSW, 2109, Australia

[5]Department of Astronomy, University of Washington, Box 351580, Seattle, WA 98195, USA; ivezic@astro.washington.edu

[6]Department of Science Education, Ewha Womans University, Seoul 120-750, Republic of Korea; deokkeun@ewha.ac.kr

[7]Astronomical Institute, Tohoku University, Sendai 980-8578, Japan; chiba@astr.tohoku.ac.jp

[8]U.S. Naval Observatory, Flagstaff Station, 10391 W. Naval Observatory Road, Flagstaff, AZ 86001, USA; jam@nofs.navy.mil

[9]INAF-Osservatorio Astronomico di Torino, via Osservatorio 20, 10025 Pino Torinese, Italy; refiorentin@oato.inaf.it

[10]Indian Institute of Astrophysics, II Block, Koramangala, Bangalore 560 034, India; sivarani@iiap.res.in

[11]Physics and Astronomy Department, University of Kentucky, Lexington, KY 40506; rjwi222@uky.edu

[12]Fermi National Accelerator Laboratory, Batavia, IL 60510, USA; yanny@fnal.gov

[13]Department of Astronomy and Astrophysics, University of Chicago, Chicago, IL 60637, USA; don@oddjob.uchicago.edu

Subject headings: Galaxy: Evolution, Galaxy: Formation, Galaxy: Halo, Galaxy: Kinematics, Galaxy: Structure, Stars: Surveys

1. Introduction

The nature of the stellar halo of the Milky Way has been debated for many decades. Among the questions that have been asked: Is the halo a monolithic structure, well-described by a simple Gaussian velocity ellipsoid? If so, is it in zero net rotation, and does that rotational character apply to all of its constituent stars? Do the stars in the halo comprise a single stellar population, with similar ages and drawn from a common metallicity distribution function (MDF)? Can the spatial distribution of the halo stars be adequately described by a single density law (power-law or otherwise)? Due to the difficulty of teasing out the properties of such a low-density component (as compared, e.g., to the bulge and disk systems), the basic data required to address these and other questions has only recently begun to arrive. Not surprisingly, multiple interpretations have emerged.

Massive new datasets from, e.g., SkyMapper (Keller et al. 2007), Gaia (Perryman et al. 2001), and eventually, LSST (Ivezić et al. 2008a), will provide definitive answers to the above questions, and of course, raise new ones. However, it is critical to address these issues with presently available data, so that the most meaningful probes of future datasets can be developed.

The two largest spectroscopic datasets available today for examination of the stellar populations of the Milky Way are the RAdial Velocity Experiment (RAVE; Steinmetz et al. 2006; Zwitter et al. 2008; Siebert et al. 2011) and the Sloan Digital Sky Survey (SDSS; York et al. 2000), in particular the subsurvey Sloan Extension for Galactic Understanding and Exploration (SEGUE; Yanny et al. 2009). The SEGUE-2 subsurvey (Rockosi et al., in preparation) has recently been publicly released as part of SDSS DR8 (Aihara et al. 2011), and will add to this bounty of information. For now, we concentrate on the information available from the previous public release from SDSS, DR7 (Abazajian et al. 2009), and in particular address the criticisms raised by Schönrich et al. (2010; S10) of the previous work of Carollo et al. (2007; C07) and Carollo et al. (2010; C10).

Note that S10 is the version of the Schönrich et al. manuscript that appeared as arXiv:1012.0842v1. In their published paper (Schönrich et al. 2011; S11), these authors chose to respond to the submitted version of the present paper, which appeared as arXiv:1104.2513v1. Due to the potential confusion over the issues raised in the two versions of the Schönrich et al. drafts, we have confined our analysis below to the version that appeared as S10; in the Appendix we briefly consider the issues raised by S11.

Carollo et al. (2007) performed a kinematic analysis (within a local volume) for a large sample of calibration stars from SDSS DR5 (Adelman-McCarthy et al. 2007), and argued for the existence of at least a two-component halo. In their view the Galactic halo comprises two broadly overlapping structural components, an inner halo and an outer halo. Note that these labels are not merely descriptors for the regions studied, but rather are labels for two individual stellar populations. These components exhibit different spatial-density profiles, stellar orbits, and stellar metallicities. It was found that the inner-halo component dominates the population of halo stars found at distances up to 10-15 kpc from the Galactic center, while the outer-halo component dominates in the region beyond 15-20 kpc. The inner halo was shown to comprise a population of stars exhibiting a flattened spatial density distribution, with an inferred axial ratio on the order

of ~ 0.6. According to C07, inner-halo stars possess generally high orbital eccentricities, and exhibit a small (or zero) net prograde rotation around the center of the Galaxy. The MDF of the inner halo peaks at [Fe/H] $= -1.6$, with tails extending to higher and lower metallicities. By comparison, the outer halo comprises stars that exhibit a more spherical spatial-density distribution, with an axial ratio ~ 0.9. Outer-halo stars possess a wide range of orbital eccentricities, exhibit a clear retrograde net rotation, and are drawn from an MDF that peaks at [Fe/H] $= -2.2$, a factor of four lower than that of the inner-halo population.

Carollo et al. (2010) used an expanded sample of calibration stars available from SDSS DR7, which included the SEGUE sample, to refine and extend the results of C07. They derived velocity ellipsoids for the inner- and outer-halo components of the Galaxy, as well as for the canonical thick-disk and the proposed metal-weak thick-disk populations. The C10 paper also considered the fractions of each component required to understand the nature of the observed kinematic behavior of the stellar populations of the Galaxy as a function of distance from the Galactic plane. Spatial-density profiles for the inner- and outer-halo populations were inferred from a Jeans Theorem analysis. The full set of calibration stars (including those outside the local volume) was used to test for the expected changes in the observed stellar MDF with distance above the Galactic plane *in situ*, due to the changing contributions from the underlying stellar populations.

Derivation of sufficiently accurate distances is a crucial required step in carrying out kinematic analyses that make use of full space motions, as these involve distances, combined with radial velocities and proper motions, in order to assemble the local velocity components of a sample. It is these distances that have been called into question by S10. In the present paper, we show that many of their objections arise from *their incorrect adoption* of a main-sequence absolute magnitude relationship from Ivezić et al. (2008b; I08) that *does not apply* for metal-poor halo stars near the main-sequence turnoff (TO), and which leads to assignments of stellar distances that strongly disagree (a shorter scale by 10-18%) with those derived using the correct relationship recommended by I08. A legitimate criticism by S10 relates to the luminosity classifications for stars of intermediate gravity (as assigned spectroscopically) used by C07 and C10, which we demonstrate below is easily corrected. We then consider a new kinematic analysis of likely outer-halo stars from C10, and demonstrate that their original claim that the halo of the Milky Way requires at least a two-component model (with the outer-halo component in net retrograde rotation and possessing a large velocity dispersion) remains intact.

This paper is outlined as follows. In Section 2 we summarize the procedures used by C07 and C10 to derive absolute magnitudes and distance estimates for their stars, which were based on those described by Beers et al. (2000) . A technique for the reassignment of (some of the) luminosity classifications for TO stars in the original C10 sample is then developed and applied. In Section 3 we compare with absolute magnitudes and distances derived by the approaches of I08 and An et al. 2011 (in preparation; A11) for stars spectroscopically classified as likely dwarfs based on their derived surface gravities, as well as with those claimed by S10. We demonstrate concordance between the distances for low-metallicity dwarf stars obtained by C10, I08, and A11, and the apparent discordance of all three of these techniques with the results of S10. In Section 4 we reanalyze the kinematics of likely outer-halo stars from the C10 dwarf sample, as well as from the full sample, including stars of dwarf, TO, and subgiant/giant luminosity classifications, and compare to the results obtained from adoption of the I08, A11, and S10 distances. Additional tests for the presence of a kinematically and/or chemically distinct outer halo in the C10 sample are discussed in Section 5. Section 6 presents a summary of further evidence in favor of a dual halo model for the Milky Way, based on other data sets from SDSS and elsewhere. Our conclusions are given in Section 7. In the Appendix, we consider the issues raised by S11 (the published version of S10).

2. Procedures Used for Absolute Magnitude and Distance Estimates

2.1. As Employed by C07 and C10

The analyses of C07 and C10 made use of distance estimates for various luminosity classes as assigned by the software pipeline employed by SDSS/SEGUE to estimate stellar atmospheric parameters based on low-resolution ($R \sim 2000$) spectroscopy and *ugriz* photometry. The SEGUE Stellar Parameter Pipeline (SSPP) assigns distances for stars under the following assumed luminosity classes – D: dwarf, TO: main-sequence turnoff, SG/G: subgiant and giant, FHB: Field Horizontal-Branch, and AGB: Asymptotic Giant Branch.[1] Details of the development, calibration, and validation of the SSPP can be found in Lee et al. (2008a,b), Allende Prieto et al. (2008), and Smolinski et al. (2011), to which we refer the interested reader.

The SSPP obtains estimates of stellar effective temperatures, $T_{\rm eff}$, with errors of determination on the order of 150 K. The surface gravity estimates returned by the SSPP are accurate, for stars other than the coolest giants, to on the order of 0.25 dex. Metallicity estimates for stars in the temperature range 4500 K $< T_{\rm eff} <$ 7000 K are accurate to on the order of 0.2 dex.

The SSPP distance estimates for various luminosity classes are based on a set of absolute magnitude relationships (using absorption and reddening-corrected Johnson V magnitudes and $B-V$ colors) calibrated to Galactic globular and open clusters, as described by Beers et al. (2000; their Table 2). As demonstrated in Beers et al. (2000), photometric distances estimated for their sample are in good agreement with distances derived from accurate Hipparcos parallaxes. Even when confined to TO stars alone (with well-examined assignment of stars into the TO class provided from previous work), the photometric distances using the Beers et al. formulae are consistent with Hipparcos distances.

The samples used by C07 and C10 were selected from the calibration stars of SDSS/SEGUE, which cover an apparent magnitude range of $15.5 < g_0 < 18.5$. In those analyses, confinement to a local sample with distances less than 4 kpc from the Sun corresponds to a g-band absolute magnitude fainter than $M_g = 2.5$, i.e., the local sample is dominated by D and TO stars. This is in contrast to the sample considered by Beers et al. (2000), which is dominated by SG/G stars.

Since the Beers et al. (2000) approach makes use of a non-SDSS photometric system, it is also necessary to employ a color transformation from the SDSS system. Zhao & Newberg (2006) derived a transformation obtained by making matches of SDSS stars with available Johnson magnitudes and colors from the HK survey of Beers and colleagues (Beers et al. 1985, 1992), as well as additional photometry of the HK sample stars obtained over the past decade (see, e.g., Beers et al. 2007, and references therein). They obtained:

$$V = g - 0.561\,(g-r) - 0.004$$
$$B - V = 0.916\,(g-r) + 0.187$$

Stars from the HK survey were used in order to specifically include stars with [Fe/H] < -1.0, which pertain to most halo stars, although the results did not differ drastically from those of Fukugita et al. (1996) that were based primarily on higher abundance stars. The color range of the matching stars sets the region of applicability of the above transformation, which is $-0.5 < g-r < 1.0$. The choice of distance estimates

[1]The FHB and AGB classes do not pertain to the sample of calibration stars used by C07 and C10, and so are not discussed further here.

based on a non-SDSS photometric system was one of necessity at the time the SSPP was put into operation, as there were no suitably calibrated fiducials based on SDSS photometry of Galactic clusters available, and the isochrones that had been developed were rather primitive. These limitations no longer apply, and future versions of the SSPP will employ alternative distance estimates based on improvements that have become available in the past year.

It should be noted that the SSPP, by design, does not identify a preferred distance estimate, leaving the choice of the appropriate luminosity classification to the user's discretion. This choice is due, in part, to the fact that the estimation of surface gravity by the SSPP has evolved with time, and may continue to do so in the future. Hence, as many users will rely, at least at some level, on log g estimates for making distance estimates based on luminosity classifications from available spectroscopic information, no "approved" distance estimate is supplied by the SSPP.

For the purpose of the analyses carried out by C07 and C10, the following spectroscopically assigned surface gravity intervals from the SSPP were used in the assignment of luminosity classifications:

- D: log $g \geq 4.0$
- TO: $3.5 \leq$ log $g < 4.0$
- SG/G: log $g < 3.5$

Estimates of log g carry errors, and one has to be concerned about the possible effects on any resulting analyses based on their adoption. For the present, this is best assessed by consideration of inferences based on samples of individual luminosity classes relative to the sample as a whole, which we discuss below.

Note that the above prescription for assignment of luminosity class does not take into account the "known" evolutionary stage of a given star, as might be inferred from the location of a star in a color-magnitude diagram expected to pertain to objects of a given age and metallicity. This uncertainty is of particular concern for stars assigned to the TO class, since an alternative assignment to the D or SG/G class could result in potentially large discrepancies in the adopted distance. This "defect" (actually a choice, given that such knowledge is at best only partially constrained with present data, and in any case relies on assumptions regarding the underlying stellar population one adopts) is one of the criticisms of the C07 and C10 work levied by S10. However, it can be readily addressed, as described below.

As part of their analysis, I08 compared absolute magnitude estimates obtained by the Beers et al. (2000) procedures with those used in their own analysis (which only applied to dwarfs). Pointing at the bottom left panel of their Fig. 21, which examined the main-sequence comparisons of Galactic clusters between the two studies, I08 concluded that "... the median offset of implied M_r evaluated in small bins of $u - g$ and $g - r$ color is -0.07 mag, with an rms of 0.06 mag". This satisfying level of agreement provided additional reason to have faith in the distances for the majority of stars in the C10 sample upon which their kinematic analysis was based. This agreement remains intact, as shown below.

2.2. A Refined Prescription for Luminosity Class Assignments

As pointed out above, refinements in luminosity class assignment require assumptions about the ages and age distributions of the population(s) to which they will be applied. For the present discussion, which turns on the nature of the stars associated by C07 and C10 with the inner- and outer-halo populations, it is

reasonable to adopt a uniformly old age, with the unavoidable caveat that not all stars of these populations may strictly adhere to this assumption.

We proceed as follows.

First, a set of theoretical log g vs. $T_{\rm eff}$ diagrams is obtained, based on the Y^2 isochrones (Demarque et al. 2004), for a population with age set to 12 Gyrs, metallicities in the range $-3.0 \leq$ [Fe/H] ≤ 0.0, and with [α/Fe] set to 0.0 for solar metallicity, [α/Fe] = +0.3 for [Fe/H] ≤ -1.0, and using a linear scaling between [Fe/H] = 0 and [Fe/H] = -1.0. We then obtain the effective temperatures at the position of the main-sequence turnoff for each model, $T_{\rm MSTO}$, and assign a "critical temperature", $T_{\rm crit}$, to be 250 K cooler than $T_{\rm MSTO}$. The offset of 250 K was chosen since, in the region of the MSTO, this roughly corresponds to the two-sigma accuracy of the estimated temperature from the SSPP, and provides a reasonable location for the base of the subgiant branch for isochrones of old, low-metallicity populations. Our purpose is to define a criterion such that a reassignment of luminosity classes can be considered for stars of intermediate gravity ($3.5 \leq \log g < 4.0$) that are cooler than $T_{\rm crit}$.

A second-order polynomial is then fit to the positions of the $T_{\rm MSTO}$ values for each model:

$$T_{\rm MSTO} = 5572 - 519.3\,[{\rm Fe/H}] - 44.3\,[{\rm Fe/H}]^2 \quad (1)$$

The critical temperature is then simply set to $T_{\rm crit} = T_{\rm MSTO} - 250$ K. This process is illustrated in Fig. 1. The critical temperature is used in order to separate intermediate-gravity stars classified as TO by C07 and C10 into either bona-fide TO stars (those with $T_{\rm eff} \geq T_{\rm crit}$) or into the D or SG/G classes (those with $T_{\rm eff} < T_{\rm crit}$) according to their surface gravity estimates, as summarized in Table 1. Note that stars with original luminosity classifications D and SG/G are not changed by this procedure.

The luminosity class reassignment procedure described above affects a total of 4514 of the original 16920 accepted stars in the C10 sample (26%). The upper left panel of Fig. 2 shows the CMD for the original assignments of C10, while the upper right panel is that obtained after the revised assignments have been applied to this same sample. The gray dots are stars with [Fe/H] > -2.0, while the red dots are stars with [Fe/H] < -2.0.[2] As can be appreciated from comparison of these two panels, stars that formerly fell into regions of the CMD that might be considered astrophysically unlikely for an old, metal-poor population have primarily moved into either the D or SG regions. The lower panels of Fig. 2 contrast the absolute magnitudes of the revised and original C10 classifications (lower left) and the corresponding derived distances (lower right).

Inspection of the upper left panel of Fig. 2 clearly shows the presence of the "spurious" TO stars in the original C10 sample, most easily seen among the [Fe/H] < -2.0 stars as the plume extending from roughly $M_r = 3.7$ to $M_r = 4.7$, over the color range $0.25 < g - i < 0.6$. Comparison with the upper right panel of this figure shows that most of these stars (51%) are reassigned to D status, with only some 10% being reassigned to SG/G status (the remaining stars, 39%, retain their original luminosity classification of TO). At low metallicity, [Fe/H] < -2.0, the fraction of reassigned TO stars to D status is 85%, while those reassigned to SG/G status comprise 14%, and only a small fraction retain their TO classification. At higher metallicities, [Fe/H] > -2.0, 44% of the TO stars are reassigned to D status, and only a small fraction are reassigned to SG/G status. The remaining stars, 56%, retain their original luminosity classification of TO.

[2]We have made use of the corrected metallicity, [Fe/H]$_C$, as described by C10, here and throughout the rest of this paper, for the quoted metallicities.

The lower left panel of Fig. 2 shows the difference in the assigned M_r absolute magnitudes that arises when one compares the revised C10 estimates with those of C10. For the TO stars that were reclassified as D stars, and with [Fe/H] > -2.0, the revised C10 determinations are fainter by a median offset of 0.08 mags (rms 0.36 mags) for $0.4 < g-i < 0.8$, while the median offset of the revised C10 absolute magnitudes is 0.30 mags (rms 0.24 mags) fainter for bluer stars in the range $g-i < 0.4$. For the TO stars that were reclassified as SG/G stars, and with [Fe/H] > -2.0, the revised C10 determinations are brighter by a median offset of 0.48 mags (rms 0.31 mags) for $0.4 < g-i < 0.8$, while the median offset of revised C10 absolute magnitudes is 0.44 mags (rms 0.22 mags) brighter for bluer stars in the range $g-i < 0.4$.

For the TO stars that were reclassified as D stars, and with [Fe/H] < -2.0, the revised C10 determinations are fainter by a median offset of 0.97 mags (rms 0.43 mags) for $0.4 < g-i < 0.8$, while the median offset of revised C10 absolute magnitudes is 0.60 mags (rms 0.25 mags) fainter for bluer stars in the range $g-i < 0.4$. For the TO stars that were reclassified as SG/G stars, and with [Fe/H] < -2.0, the revised C10 determinations are brighter by a median offset of 1.07 mags (rms 0.42 mags) for $0.4 < g-i < 0.8$, while the median offset of revised C10 absolute magnitudes is 0.63 mags (rms 0.24 mags) brighter for bluer stars in the range $g-i < 0.4$.

The lower right panel of Fig. 2 shows the fractional difference in the derived distances between the revised C10 and C10 scales. For TO stars that were reclassified as D stars, and with [Fe/H] > -2.0 and $0.4 < g-i < 0.8$, the median offset of the revised C10 distances with respect to the C10 distances is 26% (rms 9%). In the bluer range, $g-i < 0.4$, the offset increases to about 19% (rms 6%). Both revisions are in the direction that the revised C10 scale is shorter than the original C10 scale for the reclassified TO $\rightarrow$ D stars. For TO stars that were reclassified as SG/G stars, and with [Fe/H] > -2.0 and $0.4 < g-i < 0.8$, the median offset of the revised C10 distances with respect to the C10 distances is 33% (rms 16%). In the bluer range, $g-i < 0.4$, the offset decreases to about 25% (rms 11%). Both revisions are in the direction that the revised C10 scale is longer than the original C10 scale for the reclassified TO $\rightarrow$ SG/G stars.

For TO stars that were reclassified as D stars, and with [Fe/H] < -2.0 and $0.4 < g-i < 0.8$, the median offset of the revised C10 distances with respect to the C10 distances is 36% (rms 14%). In the bluer range, $g-i < 0.4$, the offset decreases to about 24% (rms 9%). Both revisions are in the direction that the revised C10 scale is shorter than the original C10 scale for the reclassified TO $\rightarrow$ D stars. For TO stars that were reclassified as SG/G stars, and with [Fe/H] < -2.0 and $0.4 < g-i < 0.8$, the median offset of the revised C10 distances with respect to the C10 distances is 65% (rms 26%). In the bluer range, $g-i < 0.4$, the offset decreases to about 34% (rms 14%). Both revisions are in the direction that the revised C10 scale is longer than the original C10 scale for the reclassified TO $\rightarrow$ SG/G stars.

It is worth considering that our reclassification procedure *assumes* that many of the stars with spectroscopically assigned surface gravities in the range $3.75 \leq \log g < 4.0$ (those significantly cooler than an inferred old-population main-sequence turnoff) are indeed metal-poor dwarfs with slightly misestimated $\log\ g$. This is certainly a conservative assumption, and errs on the side of decreasing distances for actual TO or SG/G stars to the much smaller values that would be derived if they are in fact main-sequence dwarfs. These fine adjustments require further study and verification by high-resolution spectroscopic follow-up of a sample of such stars, at a variety of metallicities and temperatures.

Note that for construction of Figures 2-8, and for the distance-scale comparisons we carry out below, it is useful to consider samples that explore the same local volumes. For simplicity, and for consistency with C07 and C10, we have selected stars with revised C10 distance estimates that satisfy $7 < R < 10$ kpc and $d < 4$ kpc as our basis sample.

2.3. Comparison Between Revised C10 and S10

The essence of the S10 complaint is that the distance scale utilized by C07 and C10 is too "long", i.e., that we have artificially inflated the estimates of stellar distances through the combination of (1) the use of misclassified TO stars (which they suggest could be D stars instead), and in particular, (2) the use of an absolute magnitude scale for the D stars that assigns luminosities to main-sequence stars which displaces them to larger-than-appropriate distances. We have shown above that the first issue is easily corrected for, and that in any case it only applies to some 14% of the total calibration stars from C10, roughly 2300 stars. Of these, 4% of the full sample (680 stars) possess the very low metalliticties (below [Fe/H] = −2.0) that strongly influence the derived properties of a proposed outer-halo population. Thus, even if there might be some impact, it is substantially diluted by the relatively small numbers of stars for which this concern exists. In any case, we have applied the correction procedures described above, carried out the luminosity classification changes for the cooler TO stars, and in the analysis below, refer to the modified sample as the revised C10 sample. The second issue turns on whether or not one should put faith in our adopted main-sequence absolute magnitude scale, which we address in detail below.

Fig. 3 shows the result of the comparison of the revised C10 determinations with those of S10. The upper left panel of this figure shows the CMD for stars with spectroscopic assignments of D ($\log g \geq 4.0$), with absolute magnitudes from the revised C10 sample. The upper right panel shows the corresponding CMD obtained using the absolute magnitudes from S10 (Eqn. 3 below). Note that in the evaluation of both relationships, the $[Fe/H]_C$ from C10 was employed, although similar results are obtained when the adopted metallicities from the SSPP ($[Fe/H]_A$) are used. The stars are color-coded to indicate metallicities above and below [Fe/H] = −2.0.

Note that S10 did make a number of changes in their adopted absolute magnitude relationship relative to Eqn. (A1) of I08, which actually serve to bring their estimated distances into closer agreement with ours. We have not attempted to recreate these adjustments in our analysis, as the corrections they apply are themselves uncertain (and in our view not entirely well-motivated, e.g., their preference for metallicities on a scale that our own analysis does not support). Thus, one should properly consider the comparisons we make here as likely to be the maximum differences that would be obtained. The apparent difference in the scatter in absolute magnitudes seen in the upper left and upper right panels is due to the fact our adopted distances are calculated based on the empirical cluster-based fits from Beers et al. (2000), taking into account spectroscopic measurements of metallicity and surface gravity in order to assign luminosity classes, while those on the right panel come from application of a simple polynomial, which naturally leads to lack of scatter.

The lower left panel of Fig. 3 shows the difference in the assigned M_r absolute magnitudes that arises when one compares the revised C10 estimates with those of S10 for stars spectroscopically classified as D stars ($\log g \geq 4.0$). For stars with [Fe/H] > −2.0, the revised C10 determinations are brighter by a median offset of 0.38 mags (rms 0.19 mags) for $0.4 < g - i < 0.8$, while the median offset of revised C10 absolute magnitudes is 0.45 mags (rms 0.20 mags) brighter for bluer stars in the range $g - i < 0.4$. The offsets are even larger for stars with [Fe/H] < −2.0. For the redder stars with $0.4 < g - i < 0.8$, the median offset of the revised C10 determinations compared with S10 is 0.45 mags (rms 0.16 mags) brighter; for bluer stars with $g - i < 0.4$, the median offset is 0.52 mags (rms 0.18 mags) brighter.

The lower right panel of this figure shows the fractional difference in the derived distances between the revised C10 and S10 scales. For stars with [Fe/H] > −2.0 and $0.4 < g - i < 0.8$, the median offset of the revised C10 distances with respect to the S10 distances is 19% (rms 10%). In the bluer range, $g - i < 0.4$,

the offset increases to about 23% (rms 11%). For stars with [Fe/H] < -2.0 and $0.4 < g-i < 0.8$, the median offset of the revised C10 distances with respect to the S10 distances is 23% (rms 10%). In the bluer range, $g-i < 0.4$, the offset is 27% (rms 11%). All distance differences are in the sense that the revised C10 scale is (as expected) longer than the S10 scale.

3. Absolute Magnitudes and Distances Based on Alternative Schemes

Since much of the discord between the conclusions reached by C10 and S10 arise from their adopted absolute magnitudes and distances, we now consider two additional approaches for obtaining estimates of these quantities. It is worth keeping in mind that these comparisons are only valid for stars that are confidently assigned D status, for which we enforce the requirement that they have spectroscopic gravity estimates assigned by the SSPP of $\log g \geq 4.0$.

3.1. The Empirical Calibration of I08

We first consider the relationship adopted by I08, as summarized by their Eqn. (A7), used in conjunction with the metallicity correction in their Eqn. (A2) and Eqn. (A3). When combined into a single equation, one obtains:

$$\begin{aligned} M_r(g-i,[\mathrm{Fe/H}]) &= -0.56 + 14.32\,x - 12.97\,x^2 \\ &\quad +6.127\,x^3 - 1.267\,x^4 + 0.0967\,x^5 \\ &\quad -1.11\,[\mathrm{Fe/H}] - 0.18\,[\mathrm{Fe/H}]^2, \end{aligned} \tag{2}$$

where $x = (g-i)$. This was the recommended final photometric parallax relationship from I08, where it is claimed to be valid (for main-sequence stars) over a wide color range ($0.2 < g-i < 4.0$).

The S10 study did not make use of the above equation, but rather, adopted an absolute magnitude relationship taken from a previous stage of the I08 analysis, given there as Eqn. (A1), and applied a metallicity correction from Eqn.(A2) and Eqn. (A3) to obtain:

$$\begin{aligned} M_r(g-i,[\mathrm{Fe/H}]) &= 1.65 + 6.29\,x - 2.30\,x^2 \\ &\quad -1.11\,[\mathrm{Fe/H}] - 0.18\,[\mathrm{Fe/H}]^2, \end{aligned} \tag{3}$$

where $x = (g-i)$.

The S10 paper argued that their adopted absolute magnitude determinations agreed better with their preferred set of isochrones (the BaSTI isochrones: Pietrinferni et al. 2004, 2006), but in fact I08 did not expect this relationship (which is from an early step in their development of the appropriate absolute magnitude prediction) to perform well for bluer stars near the main-sequence turnoff. This is a crucial limitation, as the calibration-star sample considered by C07 and C10 includes a considerable number of bluer objects – 19% of the C10 sample, for example, have $g-i < 0.4$. The fraction becomes even larger at low metallicity – 31% for [Fe/H]< -1.0, and 46% for [Fe/H]< -2.0. This relationship also does not take into account corrections for differing ages of the underlying stellar populations that were applied by I08 in

seeking a more generally useful photometric parallax method. The combination of these two effects accounts for much of the discrepancy cited by S10 in the absolute magnitudes (hence distances) used by the C07 and C10 studies.

The upper left panel of Fig. 4 shows the CMD for stars with spectroscopic assignments of D ($\log g \geq 4.0$), with absolute magnitudes assigned by the relationship adopted by S10 (Eqn. 3 above). The upper right panel shows the corresponding CMD obtained using the absolute magnitudes from Eqn. 2 above, which is the recommended relationship from I08. Note that in the evaluation of both relationships above, the $[Fe/H]_C$ from C10 was employed, although similar results are obtained when either the photometric metallicity estimates from I08 or the adopted metallicity from the SSPP ($[Fe/H]_A$) are used. The stars are color-coded to indicate metallicities above and below [Fe/H] = −2.0. Note, however, that since both procedures adopted the same metallicity correction scheme, there are *no differences* in their behavior over different intervals of [Fe/H].

The lower left panel of Fig. 4 shows the difference in the assigned M_r absolute magnitudes that arises when one compares the adopted S10 and I08 relationships. For stars with $0.4 < g - i < 0.8$, the median offset is 0.23 mags, with the S10 assignments being fainter. The difference for bluer stars with $g - i < 0.4$ range from $\sim$ 0.23 mags fainter at the red end of this interval to roughly 1.0 mags fainter at the blue end (median difference of 0.48 mags).

The lower right panel of this figure shows the fractional difference in the derived distances between S10 and I08. For redder stars with $0.4 < g - i < 0.8$, the difference amounts to no more than about 15% at the blue end of this range (median offset of 10%), but for the bluer stars with $g - i < 0.4$ the difference increases from $\sim$ 15% up to roughly 40%, with a median offset of 20%. All distance differences are in the sense that the S10 scale is shorter than the I08 scale.

3.2. The Calibrated Isochrone Approach

Distances to individual stars can also be estimated using a set of stellar isochrones, once they have been properly calibrated against the observed colors and magnitudes of stars with known distances and ages. For the present exercise, we follow the prescription in An et al. (2009b) to derive distances to individual stars employing stellar isochrones with empirical corrections on the colors (An et al. 2009a). This calibration was based on photometry from An et al. (2008) for a number of open and globular clusters, including M67 ([Fe/H] = 0.0) and M92 ([Fe/H] = −2.4), which provides metallicity-dependent color corrections in *ugriz* over the metallicity range under consideration. A full description of the isochrone calibration can be found in A11.

After correcting the photometry for dust extinction, we performed model fits over the full parameter space (with metallicity range $-3.0 \leq$ [Fe/H] $\leq +0.4$). We included *griz* photometry and the key SSPP atmospheric parameters ([Fe/H], $\log\ g$, $T_{\rm eff}$) in the model fits, and found a best-fitting model by searching for a minimum χ^2 of the fit. Note that, for consistency with the other approaches, the corrected metallicity $[Fe/H]_C$ was employed. We assumed minimum errors in the photometry of 0.01 mags for *gri* and 0.02 mags for *z*, and took conservative errors of 0.3 dex for [Fe/H], 160 K for $T_{\rm eff}$, and 0.4 dex for $\log\ g$, as characteristic errors in each of these parameters (including possible systematic scale differences between the SSPP and the models). The lower limit of [Fe/H] in the models is −3.0, so we assumed [Fe/H] = −3.0 for any stars with metallicity less than this value. This choice has a negligible impact on distance estimation, since the isochrones are insensitive to a change in the atmospheric abundances for [Fe/H] < −3.0. An age of 12 Gyr

is assumed for [Fe/H] < -1.0, while 4 Gyr is taken for [Fe/H] > -0.3, with a linearly interpolated value for metallicities between the two boundaries. Solutions for distances were dropped from further consideration in cases where either the fitting process did not converge, or if the final reduced χ^2 of a converged fit exceeded 1.2.

Unlike the original approach described by An et al. (2009b), the calibrated isochrones actually reach into the main-sequence turnoff region, thus distance estimates are available for both TO and SG stars, in addition to D stars, albeit with lower accuracy in the distance estimates. For the purpose of our present comparisons we only accepted stars with spectroscopic assignments of surface gravity $\log g \geq 4.0$. An inter-comparison of results from various color indices indicates that the internal error in the distance modulus is ~ 0.1 mag; an additional ~ 0.1 mag error is expected from the errors in age, [Fe/H], [α/Fe], and adopted E($B-V$). This suggests that the associated distance-modulus error is $\sim 0.1-0.2$ mags for individual stars. As was the case for the I08 approach, the effects of binarity are more difficult to quantify, and are not included in this error estimate (see An et al. 2007).

The upper left panel of Fig. 5 shows the CMD obtained using the absolute magnitudes from Eqn. (A1) of I08 as adopted by S10. The upper right panel shows the CMD for stars with spectroscopic assignments as D ($\log g \geq 4.0$), with absolute magnitudes assigned by the calibrated isochrone procedure of A11. Note that in the evaluation of both relationships above, the [Fe/H]$_C$ used by C10 was employed, although similar results are obtained when either the photometric metallicity estimates or the adopted metallicity from the SSPP ([Fe/H]$_A$) were used. The stars are color-coded to indicate metallicities above and below [Fe/H]$= -2.0$. As is clear from inspection of the upper right panel, the A11 procedure assigns roughly half of the spectroscopic D stars into SG/G classifications, with correspondingly brighter absolute magnitudes near M$_r \sim 3$.

The lower left panel of Fig. 5 shows the difference in the assigned M_r absolute magnitudes that arises when one compares the adopted S10 and A11 relationships for stars spectroscopically classified as D stars. For the purpose of this exercise we focus on the stars to which the A11 procedure assigns dwarf status, with absolute magnitudes M$_r > 4.0$. For stars with [Fe/H] > -2.0, the S10 determinations are fainter than those of A11 by a median offset of 0.10 mags (rms 0.09 mags) for $0.4 < g-i < 0.8$, while they are fainter by up to 0.7 mags (median offset of 0.31 mags, rms 0.15 mags) for the bluer stars with $g-i < 0.4$. The offsets are significantly larger for stars with [Fe/H] < -2.0. For the redder stars with $0.4 < g-i < 0.8$, the median offset of the S10 determinations compared with A11 is 0.24 mags (rms 0.06 mags) fainter; for bluer stars with $g-i < 0.4$, the median offset is 0.41 mags (rms 0.15 mags) fainter.

The lower right panel of this figure shows the fractional difference in the derived distances between S10 and A11 scales. For stars with [Fe/H] > -2.0 and $0.4 < g-i < 0.8$, the median offset of the S10 distances with respect to the A11 distances is only about 4% (rms 4%). In the bluer range, $g-i < 0.4$, the median offset increases to about 13% (rms 6%). For stars with [Fe/H] < -2.0 and $0.4 < g-i < 0.8$, the median offset of the S10 distances with respect to the A11 distances increases to 10% (rms 3%). In the bluer range, $g-i < 0.4$, the median offset increases to about 17% (rms 6%). All distance differences are in the sense that the S10 scale is shorter than the A11 scale.

3.3. Comparison with the C10 Dwarfs

We now compare the C10 sample, with revised TO classifications, with the calculations of I08 (Fig. 6) and with those of A11 (Fig. 7). As can be appreciated by inspection of these figures, the absolute magnitude scale for the revised C10 sample agrees well with those from both I08 and A11 (in the latter case, one can

only consider the stars considered dwarfs by the A11 procedure; see below).

The lower left panel of Fig. 6 shows the difference in the assigned M_r absolute magnitudes that arises when one compares the revised C10 estimates with those of I08 for stars spectroscopically classified as D stars. For stars with [Fe/H] > -2.0, the revised C10 determinations are brighter by a median offset of 0.21 mags (rms 0.16 mags) for $0.4 < g - i < 0.8$, while the median offset of revised C10 absolute magnitudes is 0.14 mags (rms 0.27 mags) brighter for bluer stars in the range $g - i < 0.4$. The offsets are of similar size for stars with [Fe/H] < -2.0. For the redder stars with $0.4 < g - i < 0.8$, the median offset of the revised C10 determinations compared with I08 is 0.23 mags (rms 0.15 mags) brighter; for bluer stars, the median offset is 0.13 mags (rms 0.14 mags) brighter.

The lower right panel of this figure shows the fractional difference in the derived distances between the revised C10 and I08 scales. For stars with [Fe/H] > -2.0 and $0.4 < g - i < 0.8$, the median offset of the revised C10 distances with respect to the I08 distances is 10% (rms 9%). In the bluer range, $g - i < 0.4$, the median offset is about 6% (rms 7%). For stars with [Fe/H] < -2.0 and $0.4 < g - i < 0.8$, the median offset of the revised C10 distances with respect to the I08 distances is 11% (rms 8%). In the bluer range, $g - i < 0.4$, the median offset is 6% (rms 6%). All distance differences are in the sense that the revised C10 scale is longer than the I08 scale.

Turning to Fig. 7, if we focus on the stars that are assigned dwarf status by the A11 procedure (we accomplish this by only comparing stars with derived $M_r > 4.0$), the agreement between the revised C10 estimates of absolute magnitude and distance is only slightly worse, with respect to A11, than with respect to I08.

The lower left panel of Fig. 7 shows the difference in the assigned M_r absolute magnitudes that arises when one compares the revised C10 estimates with those of A11, for stars spectroscopically classified as D. For stars with [Fe/H] > -2.0, the revised C10 determinations are brighter by a median offset of 0.31 mags (rms 0.18 mags) for $0.4 < g - i < 0.8$, while the median offset of revised C10 absolute magnitudes is 0.17 mags (rms 0.15 mags) brighter for bluer stars in the range $g - i < 0.4$. The offsets are smaller for stars with [Fe/H] < -2.0. For the redder stars with $0.4 < g - i < 0.8$, the median offset of the revised C10 determinations compared with I08 is 0.21 mags (rms 0.14 mags) brighter; for bluer stars with $g - i < 0.4$, the median offset is 0.15 mags (rms 0.12 mags) brighter.

The lower right panel of this figure shows the fractional difference in the derived distances between the revised C10 and A11 scales. For stars with [Fe/H] > -2.0 and $0.4 < g - i < 0.8$, the median offset of the revised C10 distances with respect to the A11 distances is 15% (rms 10%). In the bluer range, $g - i < 0.4$, the median offset decreases to about 8% (rms 8%). For stars with [Fe/H] < -2.0 and $0.4 < g - i < 0.8$, the median offset of the revised C10 distances with respect to the I08 distances is 10% (rms 7%). In the bluer range, $g - i < 0.4$, the median offset is 7% (rms 6%). All distance differences are in the sense that the revised C10 scale is longer than the A11 scale.

3.4. Comparison Between A11 and I08

For completeness, Fig. 8 shows the comparison between the isocohrone fitting procedure of A11 and the calculations of I08.

The lower left panel of Fig. 8 shows the difference in the assigned M_r absolute magnitudes between the A11 and I08 estimates, for stars spectroscopically classified as D (and with $M_r > 4.0$, in order to only

compare the stars considered as dwarfs by the A11 procedure). For stars with [Fe/H] > -2.0, the A11 determinations are fainter by a median offset of 0.10 mags (rms 0.08 mags) for $0.4 < g - i < 0.8$, while the median offset is 0.12 mags (rms 0.08 mags) fainter for bluer stars in the range $g - i < 0.4$. The offsets are smaller for stars with [Fe/H] < -2.0. For the redder stars with $0.4 < g - i < 0.8$, the median offset of the A11 determinations compared with I08 is 0.06 mags (rms 0.06 mags) brighter; for bluer stars with $g - i < 0.4$, the median offset is 0.10 mags (rms 0.08 mags) fainter.

The lower right panel of this figure shows the fractional difference in the derived distances between the A11 and I08 calculations. For stars with [Fe/H] > -2.0 and $0.4 < g - i < 0.8$, the median offset of the A11 distances with respect to the I08 distances is 5% (rms 4%). In the bluer range, $g - i < 0.4$, the offset is also about 5% (rms 4%). For stars with [Fe/H] < -2.0 and $0.4 < g - i < 0.8$, the median offset of the A11 distances with respect to the I08 distances is 3% (rms 3%). In the bluer range, $g - i < 0.4$, the offset is similar, about 4% (rms 4%). The distance differences are in the sense that, for the redder stars, the A11 scale is longer than that of I08, while for the bluer stars, the A11 scale is shorter than that of I08.

If we restrict our attention to the stars with [Fe/H] < -2.0, the ones that matter the most for inferences concerning an outer-halo population, we conclude from the above analysis that the I08 and A11 distance scales are compatible with one another (maximum offsets of around 5%), while the revised C10 distance scale differs (in the sense of being longer) than both the I08 and A11 scales by no more than about 10% (better for stars near the main-sequence turnoff, around 6-7%). By contrast, the S10 scale differs (in the sense of being shorter) with respect to the I08 scale by between 10% and 18% (independent of metallicity; worse for stars near the main-sequence turnoff), and similarly, between 10% and 17% (worse for stars near the main-sequence turnoff) with respect to the A11 scale. Although it is presently unknown which of these distance scales is closer to "ground truth", the greater disagreement of the S10 scale (in particular close to the main-sequence turnoff), not only with respect to the revised C10 scale, but also with respect to those of I08 and A11, suggests that it is the S10 scale that should be considered suspect, rather than the revised C10 scale.

4. A Reanalysis of Kinematics for Likely Outer-Halo Stars

We now reconsider a limited kinematic analysis for a local sample of the SDSS DR7 calibration stars following the procedures described by C10, making use of the four different sets of distance assignments discussed above for calculation of the full space motions. In order to provide a fair comparison, we apply the same local volume constraints ($7 < R < 10$ kpc and $d < 4$ kpc) to the various samples, but use the values of R and d that would be obtained for each of the different distance scales. This has the obvious result that different numbers of stars will enter into each sample. In order to maximize the contribution from proposed outer-halo stars, we choose to only include stars with [Fe/H] ≤ -2.0. Our purpose is to test the robustness of the retrograde signature that was criticized by S10, which is most evident at low metallicity.

Fig. 9 shows histograms of V_ϕ for the stars spectroscopically classified as type D in the revised C10 sample, for all ranges of $Z_{\rm max}$ (the maximum value of the distance above or below the Galactic plane reached by a given star during its orbit). The red lines shown in each panel are the two components of a model obtained by the R-Mix procedure[3] employed by C10, to which the interested reader is referred for additional details. As can be appreciated from inspection of this figure, all four of the distance calibrations

[3]http://www.math.mcmaster.ca/peter/mix/mix.html

we consider lead to distributions of V_ϕ that include asymmetric tails, which would not be expected to arise for a single-component halo. Naturally, the suggested components and significance of the splits vary from sample to sample; Table 2 summarizes these results. Column (1) lists the sample under consideration (recall that the samples differ only in their adopted distances as described above). Columns (2) and (3) list the inferred means and dispersions (and their errors) of an assumed Gaussian population for the first component of a two-component fit to the observed distribution of V_ϕ, based on the R-Mix procedure. Columns (4) and (5) list the same quantities for the second component (where required). Column (6) is the p-value of the fits to a one-component model.

The first section of Table 2 concerns the parameters of the R-Mix fits, for D stars only, associated with Fig. 9, which applies to stars at all $Z_{\rm max}$. Note that the number of dwarfs listed in the revised C10 sample is more than twice that in the other samples; this is the result of the inclusion of the reclassified TO $\rightarrow$ D described above (including a subset of the stars with $3.75 \leq \log g < 4.00$). In the other samples, only the stars with spectroscopic estimates $\log g \geq 4.0$ are included. From inspection of the table, the suggested splits from R-Mix all include a retrograde and a prograde component, and are highly statistically significant (in the sense that a one-component fit is strongly rejected). This even includes the S10 sample, although one can see that the formal derived velocity for the first component is less retrograde than found for the other samples.

Fig. 10 shows the result of a similar analysis for the four different sets of distance calibrations, but restricted to only include stars with derived estimates of $Z_{\rm max} > 5$ kpc. The samples of spectroscopically classified D stars on orbits that reach beyond 5 kpc from the disk plane is much smaller than considered for all ranges of $Z_{\rm max}$, but the fraction of likely outer-halo stars included by this cut on $Z_{\rm max}$ should be increased.

Inspection of Fig. 10 reveals some interesting differences. While the revised C10 sample (which is considerably larger than the other samples) shown in the upper left panel exhibits a clear asymmetric tail extending to negative V_ϕ, the tails of the I08 and A11 samples are weaker than previously, but located at larger negative values of V_ϕ. We judge this to be primarily the result of the smaller numbers of stars included. Of particular interest is the lower right panel, which shows the result for the S10 sample. As can be seen, if one were to accept the S10 absolute magnitude scale and corresponding distances, one would indeed be driven to interpret at least this cut on the data as well-represented by a single component, which was the essence of the argument presented by S10.

The second section of Table 2 concerns the parameters of the R-Mix fits, for D stars only, associated with Fig. 10. From inspection of the table, the suggested splits from R-Mix include a retrograde and a prograde component for the revised C10 sample, the I08 sample, and the A11 sample, all of which are highly statistically significant, but *not* for the S10 sample, which only allows for a marginally prograde one-component fit. It is revealing that the inferred prograde velocities for the second components have dropped considerably from the case that considered all values of $Z_{\rm max}$. Of course, it should be kept in mind that the restriction here, for the purpose of comparison using the D stars only, has resulted in rather small numbers of stars included for the I08, A11, and S10 subsamples. For example, the split of the A11 sample to include a highly-retrograde, low-dispersion component is presumably driven by small-number statistics.

Finally, we consider a similar set of analyses for the full revised C10 sample, including the D, TO, and SG/G classifications and their associated distances and derived space motions. Fig. 11 shows the results of this exercise for both the full range of $Z_{\rm max}$ (left panel) and the case where only stars with $Z_{\rm max} > 5$ kpc are considered. Inspection reveals the clear presence of an asymmetric tail towards negative V_ϕ in both cases,

which we associate with the outer-halo component, as also concluded by C07 and C10.

The last two sections of Table 2 apply to the samples shown in Fig. 11. As can be seen from inspection of this table, the mean velocity of the retrograde component is similar to that obtained by C10 for $Z_{\rm max} > 5$ kpc, albeit with a slightly larger formal error (-94 ± 23 km s^{-1} vs. -80 ± 13 km s^{-1}). The dispersions of the components are also similar to those obtained previously. A one-component halo is strongly rejected in both cases. In all of the above, it should be recalled that the final results given by C10 for the parameters of the various suggested populations were derived with a custom maximum-likelihood procedure, not from the R-Mix procedure described above. Hence, small differences are expected in the final derived values.

Finally, it is worth recalling that Deason et al. (2011) speculated that the retrograde signature they find for a large sample of low-metallicity SDSS BHB stars (see further discussion below) could be due to an incorrect adopted value for the LSR rotation velocity. However, from inspection of the lower portion of Table 2, one notes that significant *differences* in the mean rotational velocities appear, indicating that a velocity shear is present between the presumed underlying populations, as it is for the Deason et al. (2011) sample as well. Thus, regardless of whether one assigns physical meaning to the presence of a truly retrograde sigature associated with the outer-halo component, all indications suggest that there is indeed a difference between the rotational properties of the inner-halo and outer-halo components.

5. Additional Tests for the Presence of a Kinematically and/or Chemically Distinct Outer Halo

The limited kinematic analysis carried out above is already strong evidence for the need of more than a single-component halo for the Milky Way, and provides insight as to why a dual-halo interpretation was not supported by S10, when using their adopted absolute magnitude scale. Nevertheless, additional tests of a complex halo model that are not strongly influenced by the adopted distance scale (other than for sample selection) are useful to carry out. In this section we consider four such pieces of evidence – (1) The origin of the retrograde signature from the revised C10 D classifications as well as for the full set of D, TO, and SG/G classifications, (2) Changes in the as-observed MDF of the revised C10 sample (including stars without measured proper motions and located outside the local samples considered in the kinematic analysis), (3) The observed distribution of Galactocentric radial velocities for the well-selected sample of Blue Horizontal-Branch (BHB) stars from SDSS DR8 discussed by Xue et al. (2011), and (4) Changes in the as-observed MDF of the BHB sample over different cuts in Galactocentric distance.

5.1. Additional Evidence (1): The Origin of the Retrograde Signature

It is useful to ask if the single-halo hypothesis, e.g., a halo as described by the best-fit kinematic model from Bond et al. (2010) (and argued to be valid by S10) can be rejected even without making use of the analysis of full space motions. The gist of the difficulty with the single-halo hypothesis is the fact that the derived rotational velocity distribution is asymmetric for stars with low [Fe/H] (this asymmetry is already present for stars with [Fe/H] < -1.5, and becomes even stronger for stars with [Fe/H] < -2.0).

The fraction of low-metallicity stars with highly-retrograde motions ($V_\phi < -200$ km s^{-1}) in the SDSS/SEGUE DR7 calibration-star sample is significantly larger than for those with highly-prograde mo-

tions. For stars with [Fe/H] < -1.5 (and exploring $Z_{max} > 0$ kpc), the fraction of stars with highly-retrograde motions is 9%, compared with 4% of stars with highly-prograde motions ($V_\phi > 200$ km s^{-1}). For stars with [Fe/H] < -2.0, the fractions are 13% highly retrograde compared with 5% highly prograde. For orbits reaching to larger distances from the Galactic plane, $Z_{max} > 5$ kpc, the asymmetry is even stronger (as expected), 16% compared with 5% for [Fe/H] < -1.5, and 20% compared with 6% at [Fe/H] < -2.0. This asymmetric behavior is present even when only spectroscopically classified dwarfs are considered (Fig. 9, Fig. 10), which alleviates concerns about potential systematic distance errors associated with the other stellar classifications.

Belief in the reality of the derived asymmetry in the rotation velocities leads naturally to several important questions. For example, "Are stars in the highly-retrograde subsample different in any other measured property than the rest of sample?," and "Why do they possess such large inferred retrograde velocities?."

Fig. 12 shows that the distributions of the g-band apparent magnitudes and $g-i$ colors are very similar for the full sample and the highly-retrograde subsample (the large red squares highlight the subsample of stars with highly-retrograde motion, $V_\phi < -200$ km s^{-1}). Their distance distributions are also similar (median distances of D stars are both ~ 2.1 kpc; median distances of the D, TO, and SG/G stars are both ~ 2.5 kpc). Since these are the quantities which, by and large, drive the spectroscopic target selection, it is unlikely that spectroscopic selection effects are important in this context. The apparent structure in this figure (the discontinuity at $g = 17$) is simply the transition between the two categories of calibration stars in the sample. The spectrophotometric calibration stars cover the apparent magnitude range $15.5 < g < 17.0$, and satisfy the color ranges $0.6 < u - g < 1.2$; $0.0 < g - r < 0.6$. The telluric calibration stars cover the same color ranges as the spectrophotometric calibration stars, but at fainter apparent magnitudes, in the range $17.0 < g < 18.5$.

Although lower latitude stars (mostly arising from the SEGUE survey) are present, the stars discussed here are observed at primarily high Galactic latitudes (the median value of $|b|$ is $\sim 60^\circ$ for all subsamples considered). Any presumed rotational signature has the greatest leverage at lower latitudes. Hence, the concern that errors in the adopted distance scale have "amplified" the derived rotational velocity component is relieved somewhat by the distribution of the sample stars on the sky themselves. Instead, the origin of the derived highly-retrograde motions is primarily driven by their large (and asymmetric) measured proper motions (bottom panels of Fig. 12). The measured proper motions for the highly-retrograde subsample are much larger than the random ($\sim 3-5$ mas yr^{-1}) and systematic (< 1 mas yr^{-1}) proper motion errors. These proper motion errors were determined using a sample of ∼60,000 quasars and are robust (see Section 2.3 of Bond et al. 2010). Of course, this quasar-based analysis cannot exclude catastrophic errors (i.e., much larger than expected from quasar behavior) in a small fraction of stars due to effects such as a bad early-epoch plate, nearby bright stars with diffraction spikes, large galaxies, etc. In order to minimize these concerns, we have verified that the sky distribution of the 95 D stars (and 144 D, TO, and SG/G stars) in the highly-retrograde subsample, selected with [Fe/H] < -1.5 and $V_\phi < -200$ km s^{-1}, is similar to that for the full sample (i.e., the highly-retrograde stars do not come from an isolated small region, and issues such as chromatic differential aberration are unlikely). In addition, we have visually inspected their SDSS images, and found that essentially all are clean detections of isolated blue stars. Based on this analysis, we conclude that there is no evidence that the large observed proper motions for the highly-retrograde subsamples are due to unrecognized systematic errors.

The visually apparent difference between the distributions of the proper-motion components for the highly-retrograde subsample of stars and the rest of the sample shown in Fig. 12 can be quantified using the so-called Two Dimensional K-S test, described by Peacock (1983) (see also Press et al. 1997). Application of the 2D K-S test clearly rejects the null hypothesis that the stars identified as belonging to the highly-

retrograde tail in V_ϕ, on the basis of their derived space motions, are drawn from the sample parent population as the rest of the sample ($p \ll 0.0001$). The discussion by S10 cautioned that asymmetries in the derived azimuthal velocities might be artificially created due to a Lutz & Keller (1973) bias in the absolute magnitudes (hence distances) for a given sample, which when applied to the proper motions could lead to the presence of an extended counter-rotating tail in the distribution of V_ϕ. While the possibility of such a bias exists, our tests based on the observed proper motions alone greatly diminish the likelihood that the highly-retrograde tail could have resulted from such an effect. That is, if the retrograde signature were indeed created in the manner suggested by S10 alone (and the stars we assign to a highly-retrograde tail were otherwise identical in their kinematic properties to the rest of the low-metallicity halo stars), we would *a priori* expect their observed proper motions to be drawn from the same parent population as those *not* in the tail. This is clearly not what the data are telling us.

In summary, the selection of stars by metallicity (a spectroscopic quantity) generates a subsample with a derived asymmetric rotational velocity distribution that is primarily due to the asymmetry of the measured proper motions themselves (obtained from imaging data). Although one can always raise the issue of selection effects in the SDSS spectroscopic sample, any simple mechanism that would introduce the observed behavior seems unlikely, because spectroscopic targeting of the calibration-star sample is performed without direct knowledge of the proper motion measurements. Therefore, this interplay between the independent imaging and spectroscopic measurements is a strong argument that the asymmetric V_ϕ distribution for low-metallicity stars is real, and that it does not arise because of errors related to derived distances or other effects we are aware of.

5.2. Additional Evidence (2): The Metallicity Distribution Function of the C10 Sample with Revised Distances and Variation with Distance from the Galactic Plane

The previous analyses of C07 and C10 both concluded that the MDF of the stars in the SDSS calibration-star sample was inconsistent (for regions beyond the possible influence of the disk system) with being drawn from a location-invariant parent population, as would be demanded by the single-halo hypothesis. Here we verify that this claim remains valid, even after reassignment of a subset of the C10 TO stars into alternative luminosity classifications. This is important to check because, as noted above, the majority of these reassignments were TO $\rightarrow$ D, which clearly leads to a reduction in their typical distances.

Fig. 13 shows the as-observed MDF for the C10 sample with revised distances, for cuts on distance from the Galactic plane, |Z|. This figure exhibits strikingly similar behavior to that seen in, e.g., Fig. 20 of C10. The SDSS/SEGUE DR7 calibration stars located within 5 kpc of the plane display MDFs that are influenced primarily by the presence of the thick-disk, the metal-weak thick disk, and the proposed inner-halo populations. In the ranges of distance greater than 5 kpc, one sees a clear transition from the MDF of the proposed inner-halo population, with peak metallicity near [Fe/H] $= -1.6$, to an MDF dominated by progressively lower-metallicity stars, with a peak near [Fe/H] $= -2.2$, that are associated with the proposed outer-halo population.

From these first two additional pieces of evidence it is difficult to justify the single-halo hypothesis, either kinematically or chemically, unless other attributes (such as smooth gradients of unknown physical origin in the motions and metallicities of member stars in the SDSS/SEGUE calibration-star sample) are invoked.

5.3. Additional Evidence (3): The Distribution of Galactocentric Radial Velocities for BHB Stars from SDSS DR8 and Variation with Metallicity

The SDSS spectroscopic samples comprise a number of alternative tracers that can be used to explore the nature of the Milky Way's halo system. Among the most powerful are the BHB stars, which are intrinsically bright and numerous, and have well-calibrated photometric distances. These have already been used by a number of previous authors, including Yanny et al. (2000), Sirko et al. (2004a,b), Xue et al. (2008, 2011), Bell et al. (2010), and Deason et al. (2011), to explore various aspects of the nature of the Milky Way's stellar halo.

The Xue et al. (2011) sample from the SDSS DR8 data release is of particular value, because all of the constituent BHB stars have been classified based on carefully applied spectroscopic tests of the Balmer lines, in addition to the usual color cuts. It is a large (N > 4000 stars), well-controlled sample, with available metallicities, radial velocities, and distance estimates, that samples the inner and outer regions of the Galaxy at distances up to 80 kpc from the Galactic center.

For the purpose of our present analysis we use the distance estimates for the FHB stars reported by the SSPP, which in turn rely on the metallicity-dependent calibration of the horizontal branch adopted by Beers et al. (2000). We employ the metallicity estimate reported from the SSPP attributed to Wilhelm, Beers, & Gray (1999), which should be superior to alternative estimates for these warm stars, and is accurate to on the order of 0.25-0.3 dex. The reported radial velocities are expected to be accurate to better than 20 km s^{-1}, based on numerous previous tests.

The left-hand column of panels shown in Fig. 14 compares the distributions of Galactocentric radial velocities for two subsamples of the BHB stars in the range $5 < r < 40$ kpc (which includes roughly 90% of the full sample reported by Xue et al. 2011), after removal of stars with $|Z| < 4$ kpc (to ensure elimination of thick-disk BHB stars). The top panel, which applies to BHB stars with [Fe/H] < -2.0, shows the best-fit Gaussian (obtained from the R-Mix procedure), with a derived mean of -15 ± 2 km s^{-1} and a dispersion of 100 ± 2 km s^{-1}. R-Mix cannot reject the single-component hypothesis for this subsample. As is immediately clear from inspection of the bottom panel, the distribution of Galactocentric radial velocities for the BHB stars with [Fe/H] < -2.0 exhibits rather different behavior. We emphasize that this subsample is chosen from stars populating the same spatial distribution and having similar distances (the median distance of the [Fe/H] > -2.0 subsample is 17.5 kpc; the median distance of the [Fe/H] < -2.0 subsample is 18.8 kpc); only the metallicity cut differs. Although the R-Mix procedure strongly rejects the single-component hypothesis (with $p = 0.002$), the derived best-fit mean would be -16 ± 3 km s^{-1}, with a dispersion of 112 ± 2 km s^{-1}. In order to obtain an acceptable description of these data, R-Mix requires a two-component fit (with means of I: -54 ± 13 km s^{-1}, II: 108 ± 18 km s^{-1}, and dispersions of I: 92 ± 6 km s^{-1}, II: 70 ± 7 km s^{-1}, respectively).

The region of the Galaxy explored by the BHB stars considered here includes possible members of the Sagittarius tidal stream (see Ruhland et al. 2011), so we have carried out the same experiment as above, but with all BHB stars from plug-plates in the directions toward the two most prominent wraps of the Sgr stream removed from the analysis. The results are shown in the right-hand column of panels in Fig. 14. Although the total numbers of BHB stars are reduced, little else changes. The median distance of the [Fe/H] > -2.0 subsample is 16.8 kpc, while the median distance of the [Fe/H] < -2.0 subsample is 18.4 kpc, similar to the previous case. The best-fit Gaussian for the [Fe/H] > -2.0 subsample, obtained from the R-Mix procedure, has a mean of -16 ± 2 km s^{-1} and a dispersion of 99 ± 2 km s^{-1}. R-Mix cannot reject the single-component hypothesis for this subsample. In the case of the [Fe/H] < -2.0 subsample, the R-Mix procedure once again

rejects the single-component hypothesis (with $p = 0.02$); the derived best-fit mean would be -16 ± 3 km s^{-1}, with a dispersion of 112 $\pm$2 km s^{-1}. To obtain an acceptable description of these data, R-Mix requires a two-component fit (with means of I: -52 ± 13 km s^{-1}, II: 114 ± 19 km s^{-1}, and dispersions of I: 94 $\pm$6 km s^{-1}, II: 69 $\pm$8 km s^{-1}, respectively).

In both cases (with or without the Sgr fields included) a two-sample K-S test rejects the hypothesis that the subsamples of stars split at [Fe/H] $= -2.0$ are drawn from the same parent population at high statistical significance ($p = 0.01$ for the first instance and $p = 0.03$ in the second instance). Similarly, a parametric F-test that the dispersions are the same rejects this hypothesis in both cases, with $p < 0.001$. The observed radial velocities and metallicities of the BHB stars are telling us that the halo is not a single population.

5.4. Additional Evidence (4): The Metallicity Distribution Function of SDSS DR8 BHB Stars and Variation with Galactocentric Distance

We now reconsider evidence similar to that presented in C07, which reported an apparent variation of the nature of the MDF for horizontal-branch stars selected from SDSS DR5. Here we make use of the same sample discussed above, the BHB stars from Xue et al. (2011), which is substantially larger. As before, we have considered this sample for two instances – with and without inclusion of BHB stars from plug-plates in the directions of the Sgr tidal stream.

The left-hand column of panels in Fig. 15 shows the distribution of [Fe/H] in intervals of Galactocentric distance for the full sample, after removal of stars with $|Z| < 4$ kpc. The peak of the MDF in this panel is at [Fe/H] $= -1.7$, close to what we would associate with dominance by an inner-halo population. Comparing with the lower panels, the peak of the MDF shifts to [Fe/H] ~ -2, close to that we would associate with an outer-halo population. The strength of the low-metallicity tail in the lower panels is also clearly greater than seen in the top panel. The fractions of stars with [Fe/H] < -2.0 increase from 31% for stars with 5 $< r <$ 10 kpc to between 46% and 49% for stars at larger Galactocentric distances. Indeed, a K-S test of the null hypothesis that the MDFs of stars shown in the lower panels for the individual cuts on Galactocentric distance r could be drawn from the same parent population as the stars shown in the top panel, against an alternative that the stars are drawn from more metal-poor parent MDFs, is rejected at high levels of statistical significance (one-sided probabilities of $p < 0.001$ for all three higher cuts on Galactocentric distance).

The right-hand column of panels in Fig. 15 is similar, but with the BHB stars from plug-plates in the directions of the Sgr tidal stream removed. As can be verified by inspection, little changes. The fractions of stars with [Fe/H] < -2.0 increase from 30% for stars with $5 < r < 10$ kpc to between 44% and 48% for stars at larger Galactocentric distances. A K-S test of the null hypothesis that the MDFs of stars shown in the lower panels for the individual cuts on Galactocentric distance r could be drawn from the same parent population as the stars shown in the top panel, against an alternative that the stars are drawn from more metal-poor parent MDFs, is rejected at high levels of statistical significance (one-sided probabilities of $p < 0.001$ for all three higher cuts on Galactocentric distance), as in the previous case.

It is also interesting that the most dramatic shift in the appearance of the MDFs in both the left-hand and right-hand columns of panels shown in Fig. 15 occurs between the top panels at $5 < r < 10$ kpc, and the next larger cuts in distance, at $10 < r < 20$ kpc, and hardly changes thereafter. Indeed, a K-S test of the third distance cuts compared with the second cuts, as well as for the fourth cuts compared with the third cuts, cannot reject the hypothesis that the samples are drawn from the same parent populations. Such

a behavior might be easier to understand as a superposition of multiple populations, with different mean metallicities, rather than by invoking a continuous change that might be expected if a strong metallicity gradient were present in the halo of the Galaxy. In any event, this behavior is difficult to reconcile with the hypothesis of a single-halo population possessing a spatially invariant MDF.

6. Further Evidence for the Dual Halo of the Milky Way

Quite independent of the above discussion of the C07 and C10 calibration-star samples and the DR8 BHB sample, a substantial amount of evidence in support of the dual-halo interpretation has already appeared in the literature, or has been recently submitted for publication. Below we summarize a few of the examples we consider the most persuasive.

6.1. From Inside the SDSS

6.1.1. The SDSS DR7 BHB Sample Analyzed by Deason et al. (2011)

Deason et al. (2011) have examined a sample of BHB stars selected from SDSS DR7, using a combination of color cuts and log g and $T_{\rm eff}$ intervals from the SSPP. Their sample overlaps substantially with that used by Xue et al. (2008) to obtain estimates of the mass and constraints on the mass profile of the Milky Way, which was based on SDSS DR6 (Adelman-McCarthy et al. 2008). The Deason et al. sample is larger (by about a factor of two) than that used by Xue et al., not only due to the additional targets that were included in DR7, but also because their selection is not as restrictive.

Among other results, these authors have used a set of adopted distribution functions to model the observed Galactocentric radial velocities as a function of distance and metallicity. They found that this sample of halo stars exhibits a dichotomy between a prograde, comparatively metal-rich component ([Fe/H] > -2), and a retrograde, comparatively metal-poor ([Fe/H] < -2) component. Although these properties are quite similar to those advocated by C07 and C10, they concluded that the existence of a low-metallicity retrograde population may simply indicate that estimates of the rotation of the Local Standard of Rest (LSR), for which they adopt the IAU recommended value of 220 km s^{-1}, may be underestimated by some 20 km s^{-1}. They also point out that their results contrast somewhat with those from C07 and C10, in that *both* their retrograde and prograde populations are found in the distant regions of the halo, and are not necessarily due to a shift in stellar populations with distance from the Galactic center, as envisioned by the Carollo et al. studies. While such details demand further investigation, it is clear that the Deason et al. results would not support a single-halo interpretation of the present data.

6.1.2. Spatial Variations in the Metallicity and Density Profiles for Modeled Halo Components from de Jong et al. (2010)

During the course of the SEGUE subsurvey conducted during SDSS-II (Yanny et al. 2009), ten "vertical" (in Galactic coordinates) photometric scans of width 2.5°, crossing the Galactic plane at fixed longitudes, were imaged in the *ugriz* passbands. The purpose of these scans was to extend previous SDSS imaging to include selected areas in the latitude range $-50° < b < +50°$, and thereby obtain more detailed information on the transition from the halo system to the disk system of the Milky Way. In their analysis of these data,

de Jong et al. (2010) employed a CMD fitting approach, based on templates of old stellar populations with differing metallicities, to obtain a sparse three-dimensional map of the stellar distribution at $|Z| > 1$ kpc.

The maps of de Jong et al. (2010) provide clear *in situ* evidence for a shift in the mean metallicity of the Milky Way's stellar halo – within $r \lesssim 15$ kpc their derived stellar halo exhibited a mean metallicity of [Fe/H] ~ -1.6, changing to [Fe/H] ~ -2.2 at larger Galactocentric distances. In addition, inspection of the spatial-density profiles of their template populations (their Fig. 7) suggested rather different behaviors for their "inner-halo like" template population and that of their "outer-halo like" template population. Their derived inner-halo density profile falls off rapidly with distance from the Galactic center to $r \sim 15 - 20$ kpc; beyond this region a substantially lower density, slowly varying, outer-halo density profile was found. Note that the de Jong et al. analysis was restricted to distances $r < 30$ kpc. When a single power-law was fit to this entire region they obtained an index of $n = -2.75 \pm 0.07$, in excellent agreement with the previous work of Bell et al. (2008) and Jurić et al. (2008).

Clearly, these findings provide compelling support for the kinematics-based inferences of C07 and C10, as confirmed by our own reanalysis above, as well as by the newly-considered BHB samples.

6.1.3. Rejection of Single Power-Law Descriptions of the Milky Way's Halo based on Deep Repeated SDSS Imaging from Watkins et al. (2009) and Sesar et al. (2010)

The region known as Stripe 82 (an area of $\sim$250 deg^2 along the Celestial Equator) has been multiply scanned in the *ugriz* filters over the course of SDSS and its extensions, in particular during the Supernova Survey conducted as part of SDSS-II (Frieman et al. 2008).

Both Watkins et al. (2009) and Sesar et al. (2010) have argued persuasively that single power-law profiles are incapable of describing the spatial variation of the halo system. These authors presented evidence, based on both RR Lyrae stars and main-sequence stars, that the halo stellar number-density profile significantly steepens beyond a Galactocentric distance of $r \sim$30 kpc. It is worth noting that a "steepening" density profile might also be envisaged as describing the behavior of a profile that suffers a large drop in stellar number density at a given distance, and goes over to a more slowly varying profile with distance, as was seen in the de Jong et al. (2010) analysis.

6.1.4. The Identification of Spatial Autocorrelation in [Fe/H] based on ECHOS from Schlaufman et al. (2011)

Schlaufman et al. (2009) have described the results of a systematic, statistical search for elements of kinematically-cold halo substructure (ECHOS) amoung the inner-halo metal-poor main-sequence turnoff (MPMSTO) population identified during the course of SDSS/SEGUE. A by-product of the search for ECHOS described by these authors is a catalog of MPMSTO stars far more than 4 kpc from the Galactic plane, between 10 and 17.5 kpc from the Galactic center, and free of both surface-brightness and radial-velocity substructure, which they refer to as a 'pure smooth halo sample.' In the second paper in this series (Schlaufman et al. 2011a), they analyzed co-added MPMSTO spectra to derive the average [Fe/H] and [α/Fe] for ECHOS, as well as for the smooth component of the halo along the same line of sight as each ECHOS. They reported that the MPMSTO stars in ECHOS were systematically more metal rich and less [α/Fe] enhanced than the MPMSTO stars in the smooth component of the halo, concluding that the chemical-abundance

pattern of ECHOS was best matched by that of a massive dSph galaxy with $M_{tot} \gtrsim 10^9 M_{\odot}$.

In the third paper of the series, Schlaufman et al. (2011b) quantify the degree of spatial chemical inhomogeneity and spatial variation in chemical abundance in the smooth component of the halo, using their substructure-cleaned sample of MPMSTO stars. These authors report that the classical smooth halo component ceases to be the dominant component of the stellar population of the halo system beyond about 15 kpc from the Galactic center, and furthermore, that there exists significant spatial coherence in [Fe/H] in the MPMSTO population beyond this distance. They suggest from these findings that the relative contribution of disrupted low-mass galaxies to the stellar population of the smooth halo increases with radius, becoming observable relative to the classical kinematically smooth halo beyond 15 kpc. They also find that the morphology of the halo system in the [Fe/H]/[α/Fe] plane inside of 15 kpc is not well-matched by phased-mixed tidal debris. Instead, they argue that the smooth halo inside of 15 kpc is likely formed through a combination of *in situ* star formation and dissipative major mergers at high redshift. They conclude that their results are ... "consistent with the dual halo idea advanced in Carollo et al. (2007,2010)...".

6.2. From Outside the SDSS

Over the past several decades there have been numerous studies of the nature of the halo system that provide evidence indicating the halo of the Milky Way may not comprise a single population, based on analyses of the spatial number-density profiles of halo tracer objects (such as globular clusters or field horizontal-branch stars), and of the kinematics of small subsamples of these. Here we briefly mention a subset of these, based on data obtained outside the SDSS.

Representative spatial-analysis papers include Hartwick (1987), Sommer-Larsen & Zhen (1990; using density profiles inferred from local kinematics), Preston et al. (1991), Zinn (1993), Kinman et al. (1994), and Chiba & Beers (2000) (using density profiles inferred from local kinematics), all of which reached similar conclusions. According to these studies, the halo is best described as flattened in the inner regions, but going over to a much more spherical distribution at larger radii. Similar work has been conducted with ever increasing sample sizes in recent years. Examples include analyses of RR Lyraes based on the data from the QUEST survey (Vivas & Zinn 2006), as well as from the LONEOS sample (Miceli et al. 2008). In this latter example, Miceli et al. argued for the presence of a dual halo in order to account for the apparently very different spatial profiles of Oosterhoff Type I and Oosterhoff Type II variables in their sample. Most recently, Sesar et al. (2011) used deep imaging data from the CFHT Legacy Survey to study the distribution of near-turnoff main-sequence stars in the Galactic halo along four lines of sight, to heliocentric distances of $\sim$35 kpc. They found that the halo stellar number-density profile becomes steeper at Galactocentric distances greater than $r \sim 30$ kpc, and emphasize that single power-law models are strongly disfavored by the data.

Representative kinematical-analysis papers include Norris & Ryan (1989), Allen et al. (1991), Carney et al. (1996), Wilhelm et al. (1996), Borkova & Marsakov (2003), Kinman et al. (2007), and de Propris et al. (2010). Several of these papers (Norris & Ryan 1989; Allen et al. 1991; Carney et al. 1996) emphasized the clear presence of individual stars, in particular those with low metallicities, associated with large retrograde motions. Below [Fe/H] = -2.0, the numbers of retrograde stars in both Allen et al. (1991) and Carney et al. (1996) are well in excess of the numbers expected for fair samples drawn from a single halo population with little or no net rotation. Indeed, both sets of authors commented on the need for a complex halo in order to accommodate their observations. Wilhelm et al. (1996), Borkova & Marsakov (2003), and Kinman

et al. (2007) all reported significant net retrograde motions for subsamples drawn from their BHB and RR Lyrae star samples, respectively. Most recently, de Propris et al. (2010) have presented radial velocity data from BHB stars indicating that the velocity dispersion profile of the halo appears to increase towards large Galactocentric radii, while the stellar velocity distribution is non-Gaussian beyond 60 kpc. They concluded that the outer halo consists of a multitude of low luminosity overlapping tidal streams from recently accreted objects.

7. Summary and Conclusions

We have considered the criticisms of S10 in detail, and demonstrated that their claim that the retrograde signature of the outer-halo population is due to incorrect distance determinations or improper assignments of the stellar luminosity classes appears spurious. The original assertions of C07 and C10 are in fact confirmed by our analysis. The distance scale advocated by S10 was based on their adoption of the incorrect main-sequence absolute magnitude relationship from the work of I08. We have shown that, for redder stars, this scale is roughly 10% (in the median distance) shorter than the correct globular cluster-based scale suggested by I08, increasing to 18% shorter for bluer stars near the main-sequence turnoff, independent of metallicity. Comparison with a calibrated isochrone approach by A11 indicates that, for stars with [Fe/H] < -2.0 (which dominate the membership of the outer-halo population), the S10 scale is roughly 10% shorter for redder stars and 17% shorter for bluer stars near the main-sequence turnoff. The distance scale for main-sequence dwarfs with [Fe/H] < -2.0, based on the revised C10 classifications (including reassigned TO $\rightarrow$ D stars), agree with the determinations of both I08 and A11 at a level of 6-10%, which we consider more than adequate.

We have carried out an abbreviated kinematic analysis for the very low-metallicity stars that dominate the proposed outer-halo component, using the distance scales of the various studies considered above. Based on this analysis, we confirm the existence of a significant retrograde population (with a large velocity dispersion), which C07 and C10 associated with this structure. Furthermore, we have shown that the origin of the retrograde signature at low metallicity is traceable to the asymmetric distribution of the observed proper motions, not to the assignment of incorrect distances. The shift of the MDF for the C10 sample with distance from the Galactic plane, the distribution of Galactocentric radial velocities for BHB stars from SDSS DR8, as well as the variation of the BHB MDF with Galactocentric distance, in addition to other evidence from inside and outside the SDSS, are all consistent with a kinematically and/or chemically distinct superposition of inner- and outer-halo populations in the Milky Way, and not with a homogeneous single-halo population.

Over the span of the past quarter century, data from many independent surveys, based on very different selection criteria, distance estimation techniques, and analysis methodologies, have been pointing with ever increasing confidence to the conclusion that a single-halo description is no longer valid for the Milky Way. We have summarized the most relevant results here, although much additional evidence exists.

It is important to note that recent high-resolution, cosmologically-based simulations, in particular those of Zolotov et al. (2009, 2010), Font et al. (2011), and Tissera et al. (2011), now include at least approximate prescriptions for the star formation and dissipative accretion processes, as well as other pertinent baryonic physics such as metal-dependent cooling and supernova feedback, greatly expanding their predictive power. This new generation of simulations indicates that a dual halo (with different stellar spatial-density profiles and clear metallicity shifts between an inner- and outer-halo population) is *a generic expectation* for large spiral galaxies such as the Milky Way and M31. The Font et al. (2011) analysis emphasizes the structural characteristics of their simulations; they find remarkable similarities to the observed characteristics of the

Milky Way reported by C07, C10, and de Jong et al. (2010), including the detection of "breaks" in the stellar spatial-density profiles and metallicity drops of from 0.6 to 0.9 dex in going from the regions they associate with an inner halo to an outer halo. The Tissera et al. (2011) study emphasizes the contrasting chemical properties of the components they associate with an inner halo and outer halo in their suite of simulations, separated on the basis of the binding energy of the stellar particles. As shown in their Fig. 4, clear shifts are seen in the mean [Fe/H] of the particles in their inner/outer haloes, always in the sense that the outer halo is substantially more metal-poor than the inner halo. The median differences they obtain between these components range over $-0.4 < \Delta$[Fe/H] < -0.9, well-bracketing the difference in the peak metallicities of the Milky Way's inner halo and outer halo reported by C07 and C10 (Δ[Fe/H]$= -0.6$). Finally, the McCarthy et al. (2011) analysis of the kinematical behavior of star particles from the Font et al. (2011) simulations appears completely consistent with what might have been expected from the observational analysis of C07 and C10. We draw particular attention to their Fig. 10, which illustrates clear differences in the (velocity-dispersion scaled) rotational properties of their '*in situ* spheroid' (inner halo) and their 'accreted spheroid' (outer halo). Their Fig. 11, a representation of a Toomre diagram for their simulations, clearly indicates that their *in situ* spheroid and accreted spheroid possess strongly contrasting velocity dispersions, as also has been shown by C07 and C10 to be an observed characteristic of the halo system of the Milky Way.

Additional analyses of the SDSS/SEGUE stars, beyond those in the calibration-star subset, should help to strengthen the observational case for (at least) a dual halo, and to refine estimates of the parameters that describe the individual components. Ultimately, geometric distances from Gaia for stars in the halo populations will eliminate any remaining questions concerning the impact of uncertain photometric parallaxes on these conclusions. However, our view is that presently available data already reject the single-halo interpretation beyond reasonable doubt.

Funding for SDSS-I and SDSS-II has been provided by the Alfred P. Sloan Foundation, the Participating Institutions, the National Science Foundation, the U.S. Department of Energy, the National Aeronautics and Space Administration, the Japanese Monbukagakusho, the Max Planck Society, and the Higher Education Funding Council for England. The SDSS Web Site is http://www.sdss.org/.

The SDSS is managed by the Astrophysical Research Consortium for the Participating Institutions. The Participating Institutions are the American Museum of Natural History, Astrophysical Institute Potsdam, University of Basel, University of Cambridge, Case Western Reserve University, University of Chicago, Drexel University, Fermilab, the Institute for Advanced Study, the Japan Participation Group, Johns Hopkins University, the Joint Institute for Nuclear Astrophysics, the Kavli Institute for Particle Astrophysics and Cosmology, the Korean Scientist Group, the Chinese Academy of Sciences (LAMOST), Los Alamos National Laboratory, the Max-Planck-Institute for Astronomy (MPIA), the Max-Planck-Institute for Astrophysics (MPA), New Mexico State University, Ohio State University, University of Pittsburgh, University of Portsmouth, Princeton University, the United States Naval Observatory, and the University of Washington.

TCB and YSL acknowledge partial support from grants PHY 02-16783 and PHY 08-22648: Physics Frontiers Center/Joint Institute for Nuclear Astrophysics (JINA), awarded by the U.S. National Science Foundation. MC acknowledges support from a Grant-in-Aid for Scientific Research (20340039) of the Ministry of Education, Culture, Sports, Science and Technology in Japan. Studies at ANU of the most metal-poor populations of the Milky Way are supported by Australian Research Council grants DP0663562 and DP0984924. ZI acknowledges support from NSF grants AST 06-15991 and AST 07-07901, as well as from grant AST 05-51161 to LSST for design and development activities. DA acknowledges support provided by the National Research Foundation of Korea to the Center for Galaxy Evolution Research.

Facilities: SDSS.

A. Comments on the S11 Paper

As noted in the Introduction, we now attempt to re-establish some linearity in the progress of the discussion of the C07/C10 papers (the original presentation of the case for the presence of a dual halo for the Milky Way), the S10 criticism of these works (provided as 1012.0842v1 on the arXiv preprint server), the original Beers et al. (2011; B11) response to S10 (provided as 1104.2513v1 on the arXiv preprint server), the published version of the Schönrich et al. (2011; S11) paper, and the revised version of the B11 submission (this paper). To accomplish this, all of the remarks presented in the main body of the present paper have been confined to discussion of the S10 manuscript. Here, we offer a few responses to the issues that were raised by S11.

The S11 paper concludes in their abstract that "Finally, we note that their revised analysis presented in Beers et al. does not alleviate our main concerns." This statement is the result of S11's puzzling choice to ignore the great majority of points made by B11, including all of the substantial evidence for the presence of a dual halo *beyond those arising* from the C07/C10 analysis, which has been supplemented with additional information in Section 5 of the present paper. Furthermore, much of the S11 paper concentrates on the effect that the presence of misclassified TO stars has on the conclusions of C07/C10, even though B11 presented a set of procedures for their identification and reassignment, and demonstrated that the presence of an outer halo with properties similar to those originally claimed remains intact, even after the reassignments have been performed.

The S11 paper claims that the main-sequence relationship they adopted from I08 (Eqn. (A1) in I08, modified by S10 in ways that serve to bring it into closer agreement with Eqn. (A7) from I08 that B11 argue is the more appropriate one) is actually a reasonably accurate description of the zero-age main sequence (ZAMS) in the required color range at low metallicity. Equation (A1) was never intended to describe the ZAMS – this relationship was obtained as an intermediate step in the I08 development of their recommended absolute-magnitude relationship, Eqn. (A7). The S11 paper now claims that they find no significant differences between their analysis carried out with the modified version of Eqn. (A1) and that of Eqn. (A7), while we have shown that rather large differences can emerge (Fig. 4 of B11). Perhaps their modifications of Eqn. (A1) have corrected some of this discrepancy, but caution must still be exercised. The discussion of S11 puts a great deal of faith in their use of the BaSTI isochrones (Pietrinferni et al. 2004, 2006), using them as the basis for the statement in their conclusions that "... we have made use of direct isochone distances, which fully corroborate our findings." This statement implies that the I08 Eqn. (A7) relationship is somehow defective with respect to their choice, even though B11 demonstrate excellent agreement between the I08 Eqn. (A7) relationship and the set of *calibrated isochrones* described by A11 (Fig. 8 of B11). No mention is made in S11 of the B11 consideration of the A11 treatment.

The S11 paper (as did the S10 draft before it) makes use of the metallicity estimates from SDSS DR7, without application of the correction procedure recommended by C10, as if this correction were not needed. In fact, as several authors of C10 and B11 were responsible for assigment of the metallicities for DR7, they recognized that such a correction was required on the basis of comparison with the available high-resolution spectroscopic study of numerous low-metallicity stars. A recent verification can be found in the slides presented by Aoki (2011) at The Third Subaru International Conference on Galactic Archaeology[4]; further discussion is presented by Aoki et al. (2011, in preparation).

The S11 paper (and the S10 draft) calls attention to the possibility of the presence of a Lutz & Keller

[4]http://www.naoj.org/SubaruConf11/slides/subaru3_aokiwako.pdf

(1973) bias in distance estimates, which may give rise in turn to asymmetries in the derived azimuthal velocities. Even though a Lutz & Keller bias may exist, it cannot be responsible for the entire retrograde signature, as discussed in Section 5.1 above. Indeed, S11 neglects to address the objection noted in B11 (and expanded upon on the present paper) that consideration of the proper-motion components alone, for the stars identified as belonging to the highly- retrograde tail of the outer-halo population, are clearly not drawn from the same parent population as other stars of similarly low metallicity (Fig. 12 of B11).

In their conclusions, S11 make the assertion that the revised outer-halo mean velocity has changed from -158 km s^{-1} (pointing to Table 1 from C10) to -59 ± 20 km s^{-1} in Table 2 of B11. In fact, this apparent disagreement is spurious. Table 1 of C10 does not present the final result of C10, but rather gives results for a robust clustering analysis of V_ϕ, which applies to all stars satisfying the listed cuts, including the misclassified TO stars, and does not make use of any of the models or analysis methods of C10. Table 2 of B11 refers to an R-Mix analysis of the spectroscopically assigned D stars; the resulting net motion is in fact statistically consistent with that obtained by the maximum-likelihood result for the outer-halo component provided in Table 5 of C10, -80 ± 13 km s^{-1}; the error bars – derived in different ways – overlap at the one-sigma level. The level of agreement with the C10 result is apparently even better if one specifies to the lower portion of Table 2 of B11, which uses the (larger) full set of D, TO, and SG/G stars: -94 ± 23 km s^{-1}.

Finally, in their conclusions, S11 have mischaracterized the result of the luminosity reclassifications of the TO stars carried out by B11, claiming "... moving a considerable fraction of the wrongly identified TO stars up to the subgiant/giant branch will make the distance overestimate for the misidentified dwarfs among them even more severe". This statement is made in spite of the fact that, in Section 2.2 of B11, it is made clear that 85% of TO stars with [Fe/H] < -2.0 are reassigned to D status, while those reassigned to SG/G status only comprise 14%. The impression given to the reader by S11 would appear to be that just the opposite has occurred.

REFERENCES

Abazajian, K. N., Adelman-McCarthy, J. K., Agüeros, M. A., et al. 2009, ApJS, 182, 543

Adelman-McCarthy, J. K., Agüeros, M. A., Allam, S. A., et al. 2007, ApJS, 172, 634

Adelman-McCarthy, J. K., Agüeros, M. A., Allam, S. A., et al. 2008, ApJS, 175, 297

Aihara, H., Allende Prieto, C., An, D., et al. 2011, ApJS, 193, 29

Allen, C. A., Poveda, A., & Schuster, W. J. 1991, A&A, 244, 280

Allende Prieto, C., Sivarani, T., Beers, T. C., et al. 2008, AJ, 136, 2070

An, D., Terndrup, D. M., Pinsonneault, M. H., et al. 2007, ApJ, 655, 233

An, D., Johnson, J. A., Clem, J. L., et al. 2008, ApJS, 179, 326

An, D., Pinsonneault, M. H., Masseron, T., et al. 2009a, ApJ, 700, 523

An, D., Johnson, J. A., Beers, T. C., et al. 2009b, ApJ, 707, L64

Beers, T. C., Preston, G. W., & Shectman, S. A. 1985, AJ, 90, 2089

Beers, T. C., Preston, G. W., & Shectman, S. A. 1992, AJ, 103, 1987

Beers, T. C., Chiba, M., Yoshii, Y., et al. 2000, AJ, 119, 2866

Beers, T. C., Flynn, C., Rossi, S., et al. 2007, ApJS, 168, 128

Beers, T. C., Carollo, D., Ivezić, Ž., et al. 2011, arXiv: 1104.2513v1 (B11)

Bell, E. F., Zucker, D. B., Belokurov, V., et al. 2008, ApJ, 680, 295

Bell, E. F., Xue, X. X., Rix, H. -W., Ruhland, C., & Hogg, D. W. 2010, AJ, 140, 1850

Bond, N. A., Ivezić, Ž., Sesar, B., et al. 2010, ApJ, 716, 1

Borkova, T. V., & Marsakov, V. A. 2003, A&A, 398 133

Carney, B. W., Laird, J. B., Latham, D. W., & Aguilar, L. A. 1996, AJ, 112, 668

Carollo, D., Beers, T. C., Lee, Y. S., et al. 2007, Nature, 450, 1020 (C07)

Carollo, D., Beers, T. C., Chiba, M., et al. 2010, ApJ, 712, 692 (C10)

Chiba, M., & Beers, T. C. 2000, AJ, 119, 2843

Deason, A. J., Belokurov, V., & Evans, N. W. 2011, MNRAS, 411, 1480

de Jong, J. T. A., Yanny, B., Rix, H. -W., et al. 2010, ApJ, 714, 663

Demarque, P., Woo, J.-H., Kim, Y.-C., & Yi, S. K. 2004, ApJS, 155, 667

de Propris, R., Harrison, C. G., & Mares, P. J. 2010, ApJ, 719, 1582

Font, A. S., McCarthy, I. G., Crain, R. A., et al. 2011, MNRAS, 416, 2802

Frieman, J. A., Bassett, B., Becker, A., et al. 2008, AJ, 135, 338

Fukugita, M., Ichikawa, T., Gunn, J. E., et al. 1996, AJ, 111, 1748

Hartwick, F. D. A. 1987, in The Galaxy, NATO ASI Series 207, p. 281

Ivezić, Ž., Tyson, J. A., Allsman, R., et al. 2008a, arXiv:0805.2366

Ivezić, Ž., Sesar, B., Jurić, M., et al. 2008b, ApJ, 684, 287 (I08)

Jurić, M., Ivezić, Ž., Brooks, A., et al. 2008, ApJ, 673, 864

Keller, S. C., Schmidt, B. P., Bessell, M. S., et al. 2007, PASA, 24, 1

Kinman, T. D., Suntzeff, N. B., & Kraft, R. P. 1994, AJ, 108, 1722

Kinman, T. D., Cacciari, C., Bragaglia, A., Buzzoni, A., & Spagna, A. 2007, MNRAS, 371, 1381

Lee, Y. S., Beers, T. C., Sivarani, T., et al. 2008a, AJ, 136, 2022

Lee, Y. S., Beers, T. C., Sivarani, T., et al. 2008b, AJ, 136, 2050

Lutz, T. E., & Keller, D. H. 1973, PASP, 85, 573

McCarthy, I. G., Font, A. S., Crain, R. A., et al. 2011, MNRAS, in press, arXiv:1111.1747

Miceli, A., Rest, A., Stubbs, C. W., et al. 2008, ApJ, 678, 865

Norris, J. E., & Ryan, S. G. 1989, ApJ, 336, L17

Peacock, J. A. 2008, MNRAS, 202, 615

Perryman, M. A. C., de Boer, K. S., Gilmore, G., et al. 2001, A&A, 369, 339

Pietrinferni, A., Cassisi, S., Salaris, M., & Castelli F. 2004, ApJ, 612, 168

Pietrinferni, A., Cassisi, S., Salaris, M., & Castelli F. 2006, ApJ, 642, 797

Press W., Teukolski S., Vetterling W., & Flannery B., 1997, Numerical Recipes in C: The Art of Scientific Computing, (Cambridge Univ. Press, Cambridge), p. 645

Preston, G. W., Shectman, S. A., & Beers, T. C. 1991, ApJ, 375, 121

Ruhland, C., Bell, E. F., Rix, H.-W., & Xue, X. X. 2011, ApJ, 731, 119

Schlaufman, K. C., Rockosi, C. M., Allende Prieto, C., et al. 2009, ApJ, 703, 2177

Schlaufman, K. C., Rockosi, C. M., Lee, Y. S., Beers, T. C., & Allende Prieto, C. 2011a, ApJ, 734, 49

Schlaufman, K. C., Rockosi, C. M., Lee, Y. S., et al. 2011b, ApJ, submitted

Schönrich, R., Asplund, M., & Casagrande, L. 2010, arXiv:1012.0842v1 (S10)

Schönrich, R., Asplund, M., & Casagrande, L. 2011, MNRAS, 415, 3807 (S11)

Sesar, B., Ivezić, Ž, Grammer, S. H., et al. 2010, ApJ, 708, 717

Sesar, B., Jurić, M., & Ivezić, Ž, 2011, ApJ, 731, 4

Siebert, A., Williams, M. E. K., Siviero, A., et al. 2011, AJ, 141, 187

Sirko, E., et al., Goodman, J., Knapp, G. R., et al., 2004a, AJ, 127, 899

Sirko, E., et al., Goodman, J., Knapp, G. R., et al., 2004b, AJ, 127, 914

Sommer-Larsen, J., & Zhen, C. 1990, MNRAS, 242, 10

Smolinski, J. P., Lee, Y. S., Beers, T. C., et al. 2011, AJ, 141, 89

Steinmetz, M., Zwitter, T., Siebert, A., et al. 2006, AJ, 132, 1645

Tissera, P. B., White, S. D. M., & Scannapieco, C. 2011, MNRAS, in press, arXiv:1110.5864

Vivas A. K. & Zinn R., 2006, AJ, 132, 714

Watkins, L. L., Evans, N. W., Belokurov, V., et al. 2009, MNRAS, 398, 1757

Wilhelm, R., Beers, T. C., & Gray,. R. O. 1999, AJ, 117, 2308

Wilhelm, R., Beers, T. C., Kriessler, J. R., et al. 1996, in Formation of the Galactic Halo ... Inside and Out, ASP Conf. Ser. 92, p. 171

Xue, X. X., Rix, H. -W., Zhao, G., et al. 2008, ApJ, 684, 1143

Xue, X. X., Rix, H. -W., Yanny, B., et al., 2011, ApJ, 738, 79

Yanny, B., Newberg, H. J., Kent, S., et al. 2000, ApJ, 540, 825

Yanny, B., Rockosi, C., Newberg, H. J., et al. 2009, AJ, 137, 4377

York, D. G., Adelman, J., Anderson, J. E., et al. 2000, AJ, 120, 1579

Zhao, C., & Newberg, H. 2006, arXiv:0612.034

Zinn, R. 1993, in The Globular Clusters-Galaxy Connection, ASP Conf. Ser. 48, p. 38

Zolotov, A., Willman, B., Brooks, A. M., et al., 2009, ApJ, 702, 1058

Zolotov, A., Willman, B., Brooks, A. M., et al., 2010, ApJ, 721, 738

Zwitter, T., Siebert, A., Munari, U., et al. 2008, AJ, 136, 421

This preprint was prepared with the AAS LaTeX macros v5.2.

Table 1. Luminosity Class Refinements for Main-Sequence Turnoff Stars

Former Class	$T_{\rm eff}$ Range	Gravity Interval	New Class
TO	$\geq T_{\rm crit}$	$3.75 \leq \log g < 4.00$	TO
TO	$\geq T_{\rm crit}$	$3.50 \leq \log g < 3.75$	TO
TO	$< T_{\rm crit}$	$3.75 \leq \log g < 4.00$	D
TO	$< T_{\rm crit}$	$3.50 \leq \log g < 3.75$	SG/G

Table 2. R-Mix Results for the Low-Metallicity Subsample: Kinematic Parameters

Sample	Number	$\langle V_{\phi,I} \rangle$ (km s^{-1})	$\sigma_{V_{\phi,I}}$ (km s^{-1})	$\langle V_{\phi,II} \rangle$ (km s^{-1})	$\sigma_{V_{\phi,II}}$ (km s^{-1})	*p-value* 1-Comp
Spectroscopically Identified Dwarfs						
[Fe/H] < -2.0 ; $Z_{\rm max} > 0$ kpc						
Rev. C10	1298	-77 ± 57	117 ± 15	44 ± 11	79 ± 10	< 0.001
I08	635	-84 ± 66	94 ± 21	53 ± 20	72 ± 8	< 0.001
A11	360	-100 ± 28	124 ± 11	52 ± 12	70 ± 8	< 0.001
S10	694	-46 ± 47	85 ± 11	72 ± 14	64 ± 8	< 0.001
[Fe/H] < -2.0 ; $Z_{\rm max} > 5$ kpc						
Rev. C10	469	-59 ± 20	147 ± 11	8 ± 10	78 ± 11	< 0.001
I08	184	-200 ± 40	83 ± 28	20 ± 8	84 ± 6	< 0.001
A11	173	-395 ± 15	35 ± 12	-24 ± 12	116 ± 9	< 0.001
S10	119	13 ± 7	92 ± 5	···	···	0.8
All Stars – D, TO, and SG/G						
[Fe/H] < -2.0 ; $Z_{\rm max} > 0$ kpc						
Rev. C10	1471	-91 ± 23	124 ± 8	40 ± 9	80 ± 7	< 0.001
[Fe/H] < -2.0 ; $Z_{\rm max} > 5$ kpc						
Rev. C10	577	-94 ± 23	153 ± 9	12 ± 10	83 ± 10	< 0.001

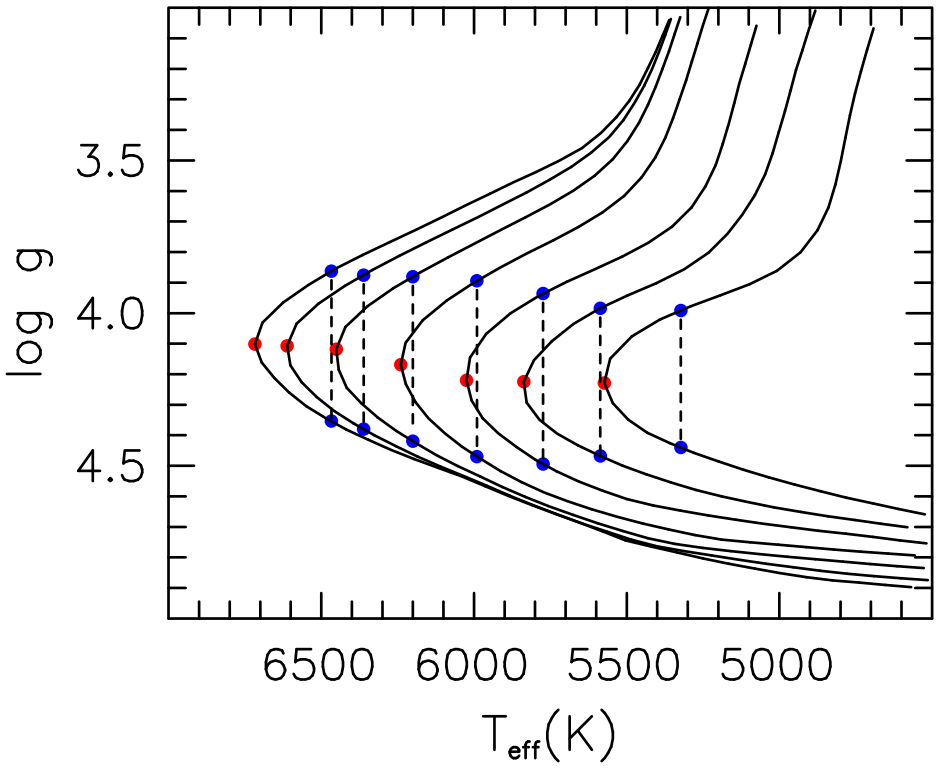

Fig. 1.— Theoretical surface gravity ($\log g$) vs. $T_{\rm eff}$ diagram based on the Y^2 isochrones (Demarque et al. 2004), under the assumption of a uniform age of 12 Gyrs. From left to right in the figure, the isochrones cover the range of metallicities $-3.0 <$ [Fe/H] < 0.0, in steps of 0.5 dex. The [α/Fe] ratios are set to 0.0 for solar metallicity, [α/Fe] $= +0.3$ for [Fe/H] ≤ -1.0, and are linearly scaling between [Fe/H] $= 0$ and [Fe/H] $= -1.0$. The red dots mark the position of the MSTO, while the blue dots correspond to temperatures 250 K cooler than the MSTO, referred to as $T_{\rm crit}$. The vertical dashed lines connect the multi-valued positions on the isochrones at a given $T_{\rm eff}$. Stars with estimated gravities in the range $3.5 \leq \log\ g < 4.0$, which were classified as TO by C07 and C10, are reassigned to either D or SG/G classes if their metallicities and $T_{\rm eff}$ place them to the right side of these divisions, or remain classified as TO if their metallicities and $T_{\rm eff}$ place them to the left of these divisions. See text for additional details.

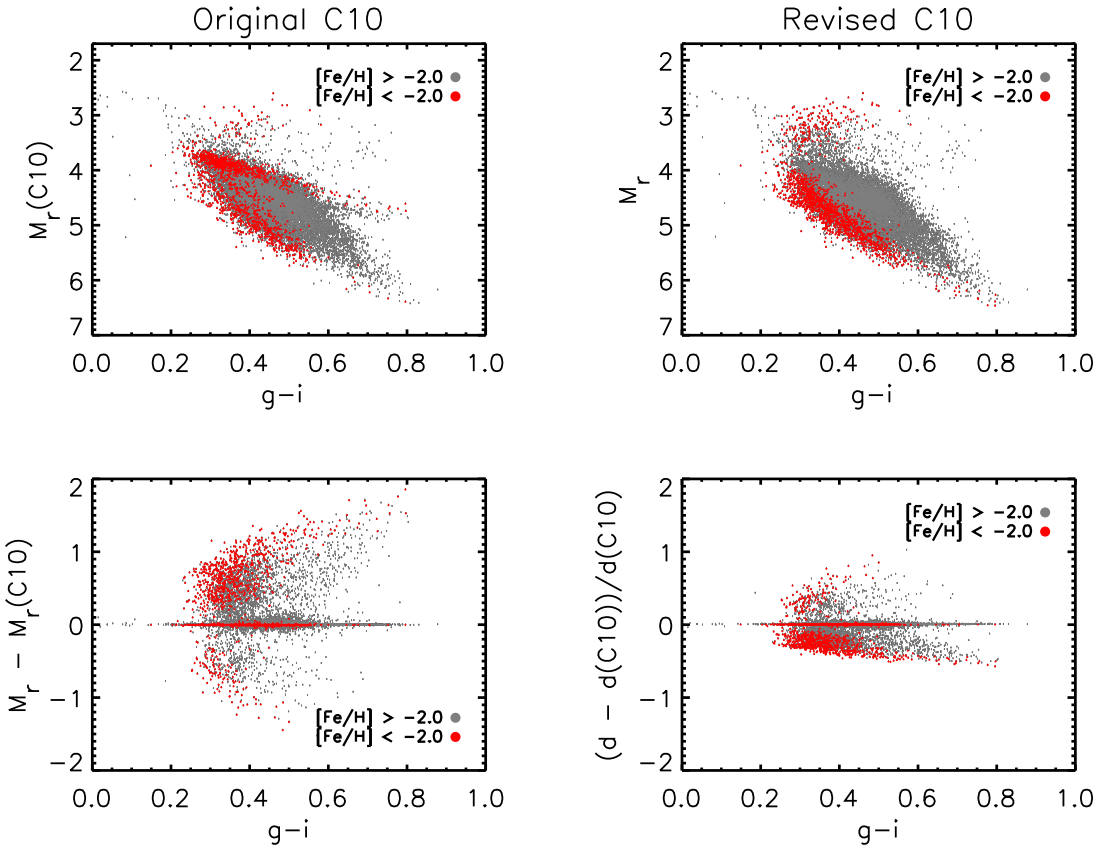

Fig. 2.— *Upper left:* $M_r, g-i$ CMD for the C10 sample, using the original luminosity classifications. *Upper right*: $M_r, g-i$ CMD for the C10 sample, using the revised luminosity classifications, as described in the text. The stars with [Fe/H] > -2.0 are shown as gray dots, while those with [Fe/H] < -2.0 are shown as red dots. *Lower left*: Difference between the M_r absolute magnitudes for the revised luminosity classifications and the original C10 classifications, as a function of $g-i$. *Lower right*: Fractional change in derived distances for the revised luminosity classifications vs. the original C10 classifications, as a function of $g-i$.

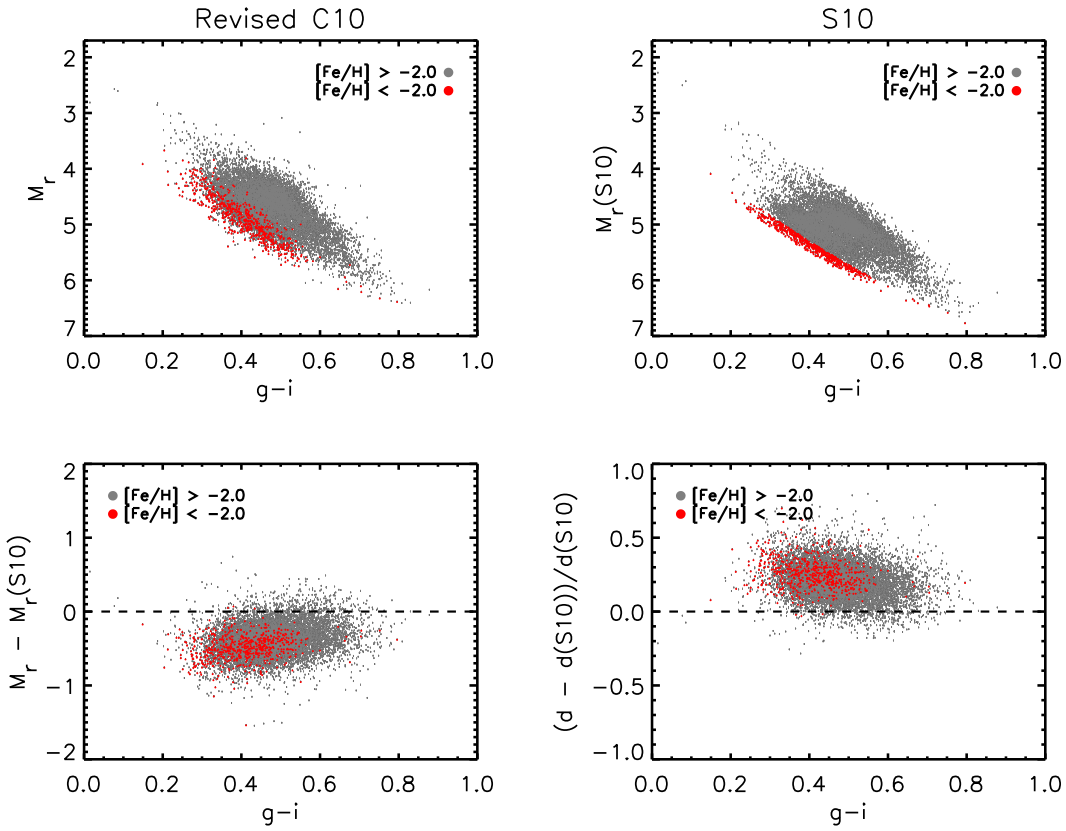

Fig. 3.— *Upper left*: $M_r, g-i$ CMD for the revised C10 luminosity classifications and with spectroscopically assigned D classifications. *Upper right*: $M_r, g-i$ CMD for stars with spectroscopically assigned D classifications, with absolute magnitudes calculated from Eqn. (A1) of I08, as adopted by S10. The stars with [Fe/H] > -2.0 are shown as gray dots, while those with [Fe/H] < -2.0 are shown as red dots. *Lower left*: Difference between the M_r absolute magnitudes for stars with spectroscopically assigned D classifications for the revised C10 and S10 calculations, as a function of $g-i$. *Lower right*: Fractional change in derived distances from the revised C10 sample as compared to those adopted by S10, as a function of $g-i$.

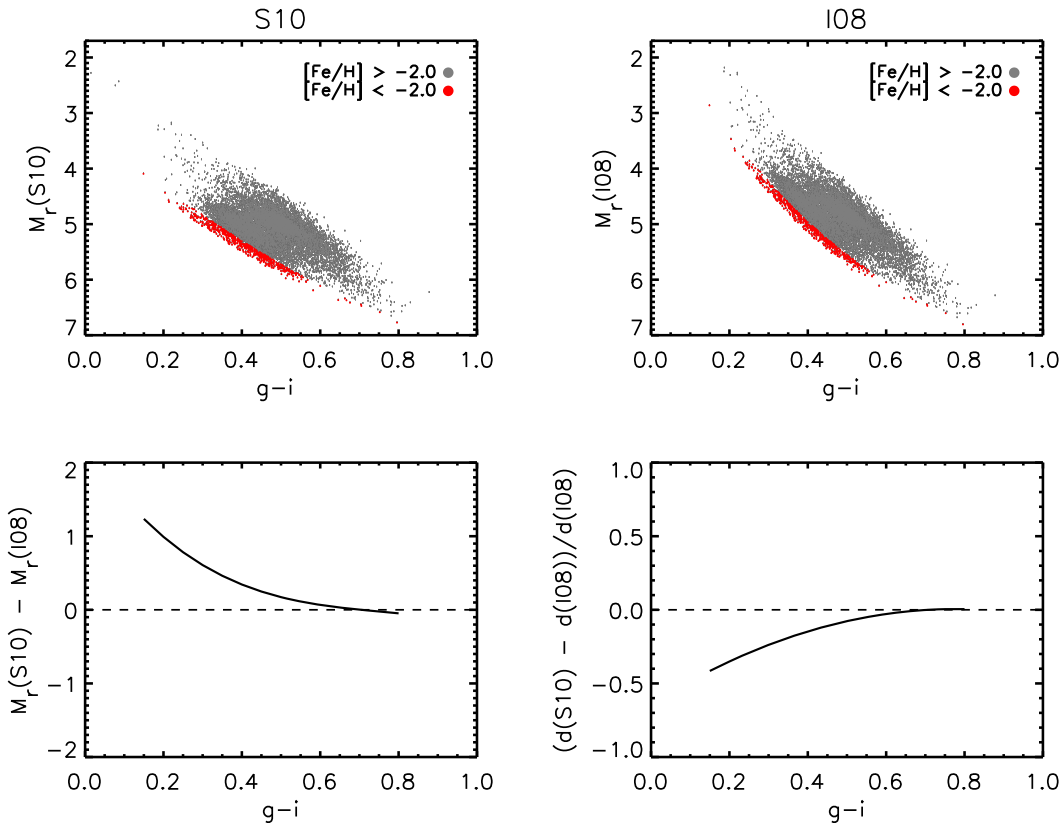

Fig. 4.— *Upper left*: $M_r, g-i$ CMD for stars with spectroscopically assigned D classifications, with absolute magnitudes calculated from Eqn. (A1) of I08, as adopted by S10. *Upper right*: $M_r, g-i$ CMD for stars with spectroscopically assigned D classifications, with absolute magnitudes calculated from Eqn. (A7) of I08, as adopted by I08. The stars with [Fe/H] > -2.0 are shown as gray dots, while those with [Fe/H] < -2.0 are shown as red dots. *Lower left*: Difference between the M_r absolute magnitudes for stars with spectroscopically assigned D classifications for the S10 and I08 calculations, as a function of $g-i$. *Lower right*: Fractional change in derived distances from those adopted by S10 as compared to those adopted by I08, as a function of $g-i$.

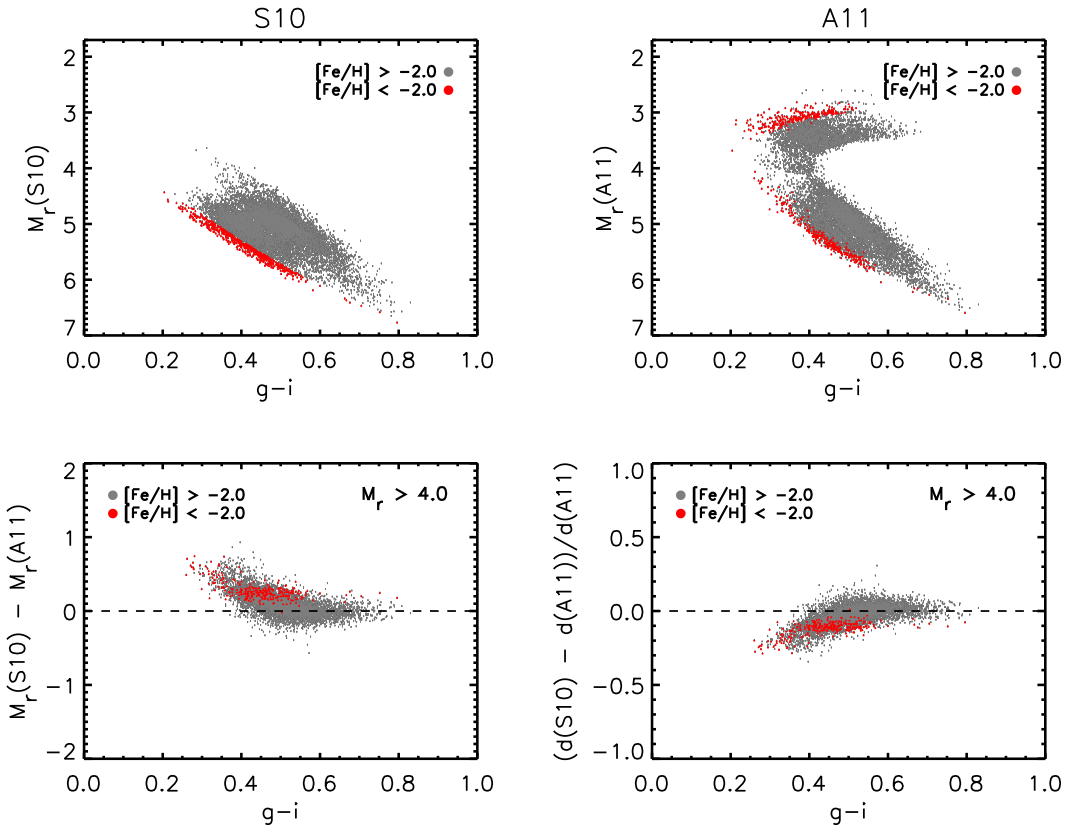

Fig. 5.— *Upper left*: $M_r, g-i$ CMD for stars with spectroscopically assigned D classifications, with absolute magnitudes calculated from Eqn. (A1) of I08, as adopted by S10. *Upper right*: $M_r, g-i$ CMD for stars with spectroscopically assigned D classifications, with absolute magnitudes calculated using the calibrated isochrone fitting procedures of A11. The stars with [Fe/H] > -2.0 are shown as gray dots, while those with [Fe/H] < -2.0 are shown as red dots. *Lower left*: Difference between the M_r absolute magnitudes for stars with spectroscopically assigned D classifications for the S10 and A11 calculations, as a function of $g-i$. *Lower right*: Fractional change in derived distances from those adopted by S10 as compared to those adopted by A11, as a function of $g-i$.

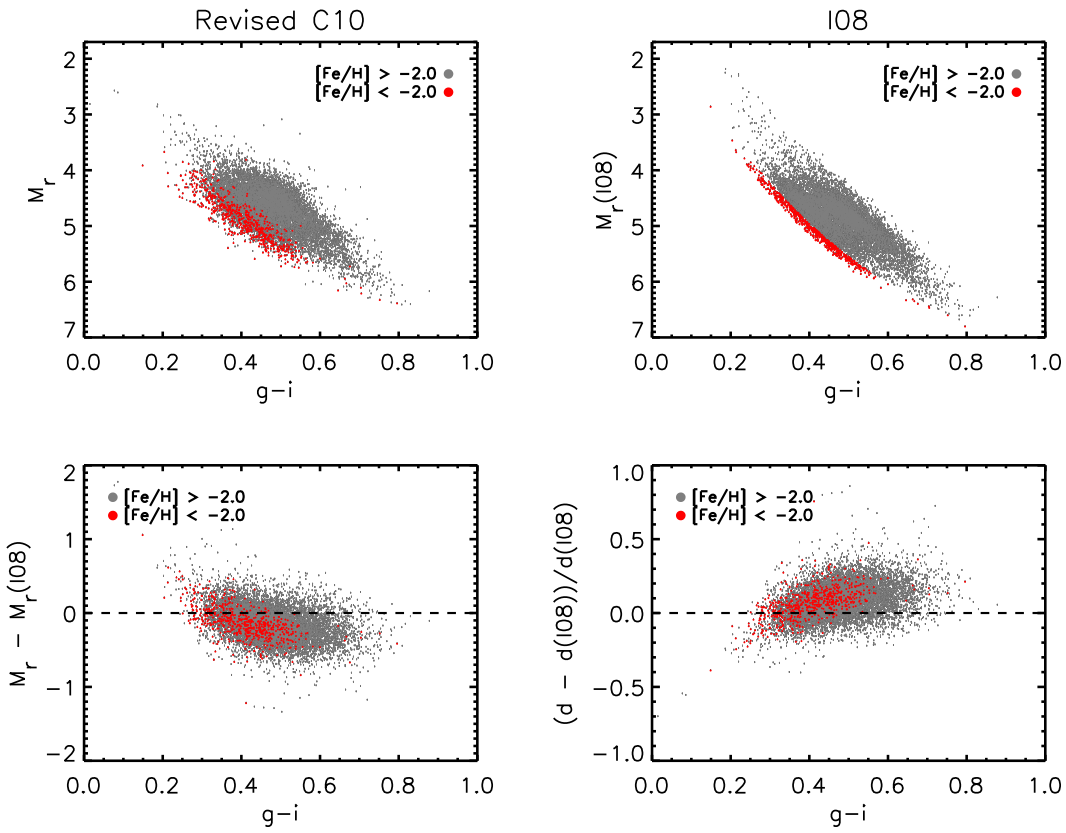

Fig. 6.— *Upper left*: $M_r, g-i$ CMD for stars with revised C10 luminosity classifications and with spectroscopically assigned D classifications, as a function of $g-i$. *Upper right*: $M_r, g-i$ CMD for stars with spectroscopically assigned D classifications, with absolute magnitudes calculated from Eqn. (A7) of I08, as adopted by I08. The stars with [Fe/H] > -2.0 are shown as gray dots, while those with [Fe/H] < -2.0 are shown as red dots. *Lower left*: Difference between the M_r absolute magnitudes for stars with spectroscopically assigned D classifications for the A11 and I08 calculations, as a function of $g-i$. *Lower right*: Fractional change in the revised distances from C10 as compared to those adopted by I08, as a function of $g-i$.

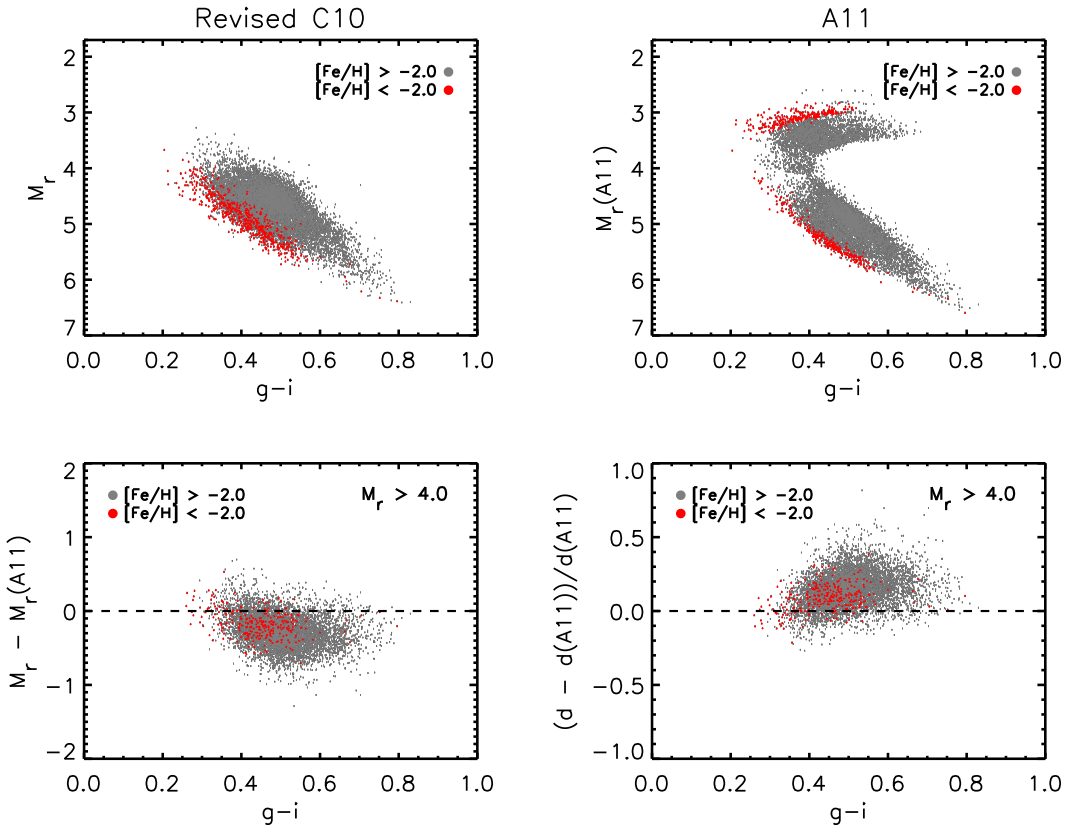

Fig. 7.— *Upper left*: $M_r, g-i$ CMD for stars with revised C10 luminosity classifications and with spectroscopically assigned D classifications, as a function of $g-i$. *Upper right*: $M_r, g-i$ CMD for stars with spectroscopically assigned D classifications, with absolute magnitudes calculated from Eqn. (A7) of I08, as adopted by I08. The stars with [Fe/H] > -2.0 are shown as gray dots, while those with [Fe/H] < -2.0 are shown as red dots. *Lower left*: Difference between the M_r absolute magnitudes for stars with spectroscopically assigned D classifications for the revised C10 and A11 calculations, as a function of $g-i$. *Lower right*: Fractional change in the revised distances from C10 as compared to those adopted by A11, as a function of $g-i$.

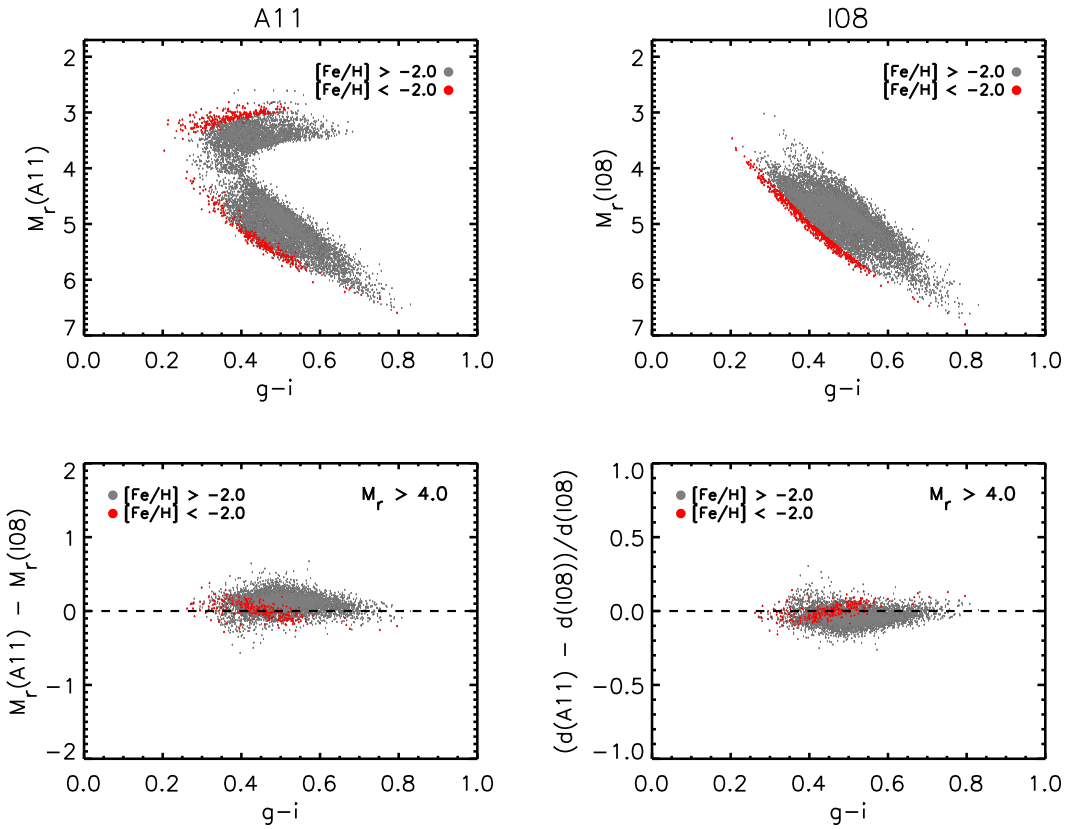

Fig. 8.— *Upper left*: $M_r, g-i$ CMD for stars with for stars with spectroscopically assigned D classifications, with absolute magnitudes calculated using the calibrated isochrone fitting procedures of A11. *Upper right*: $M_r, g-i$ CMD for stars with spectroscopically assigned D classifications, with absolute magnitudes calculated from Eqn. (A7) of I08, as adopted by I08. The stars with [Fe/H] > -2.0 are shown as gray dots, while those with [Fe/H] < -2.0 are shown as red dots. *Lower left*: Difference between the M_r absolute magnitudes for stars with spectroscopically assigned D classifications for the A11 and I08 calculations, as a function of $g-i$. *Lower right*: Fractional change in derived distances from those adopted by A11 as compared to those adopted by I08, as a function of $g-i$.

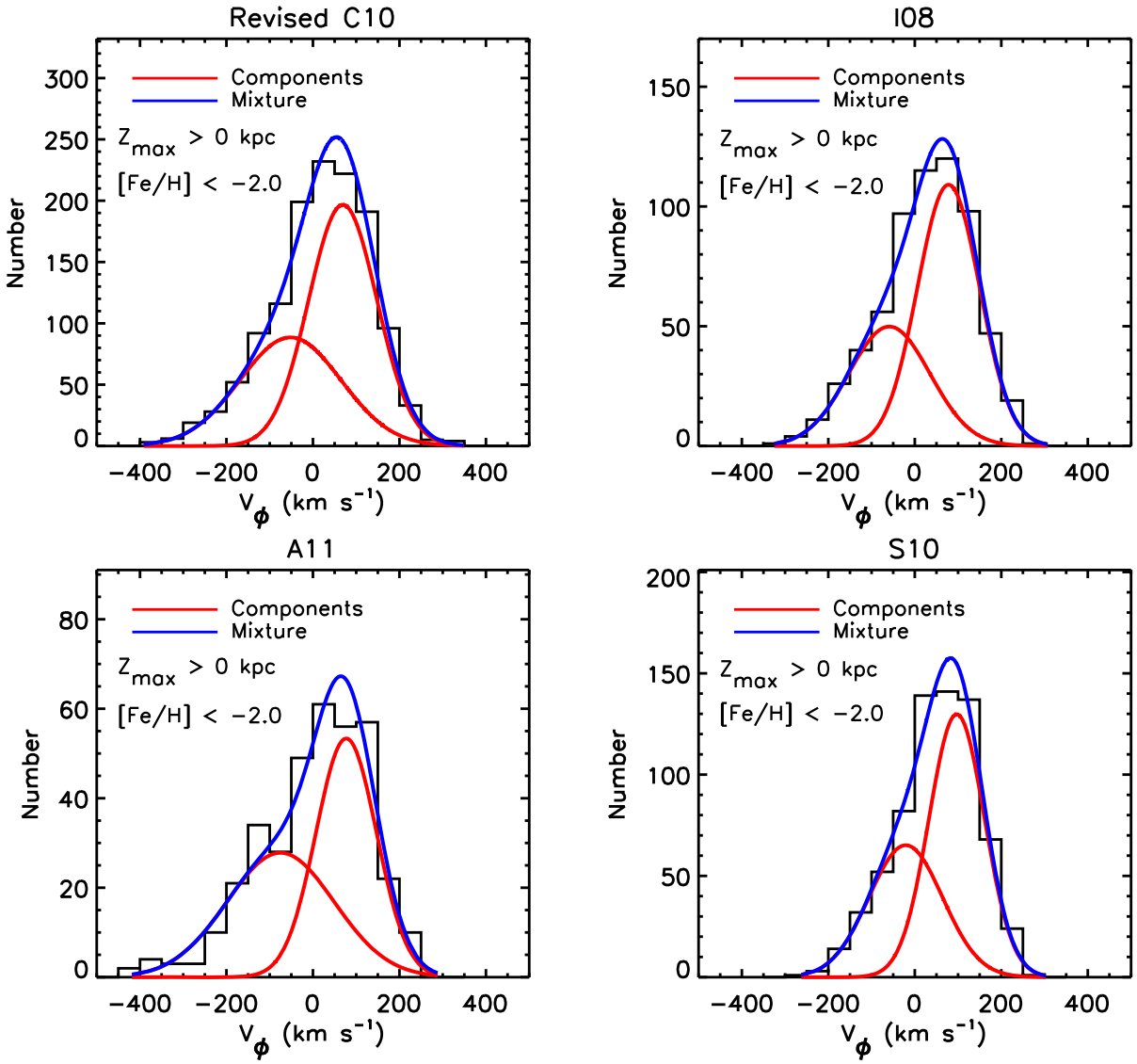

Fig. 9.— *Upper left*: Histogram of V_ϕ for stars with revised C10 distances, with spectroscopically assigned D classifications, [Fe/H] < -2.0, and all values of $Z_{\rm max}$. The red solid lines are the suggested components from the R-Mix procedure, while the blue solid line is the final mixture model. *Upper right*: Similar, for D stars with I08 distances. *Lower left*: Similar, for D stars with A11 distances. *Lower right*: Similar, for D stars with S10 distances.

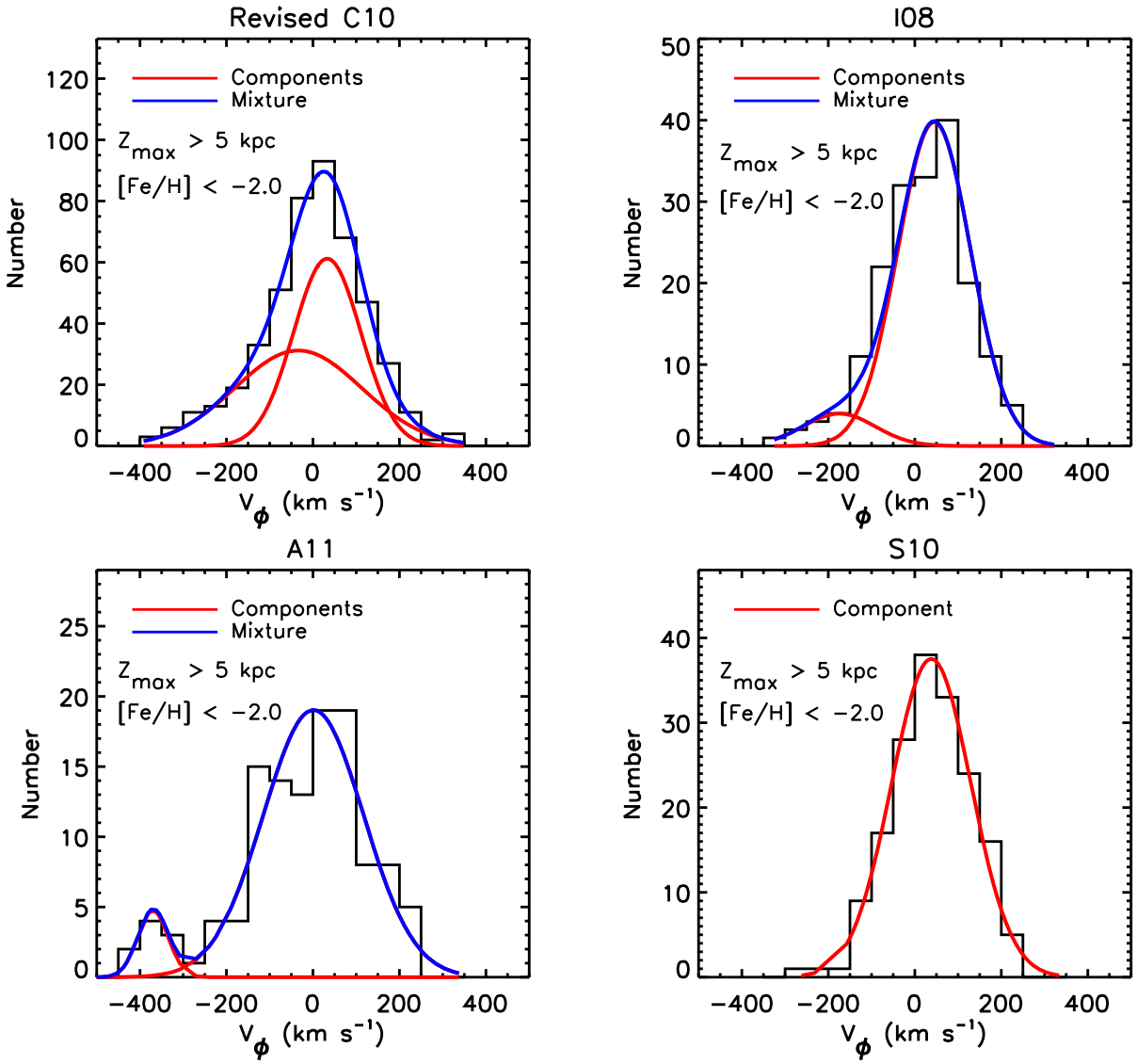

Fig. 10.— *Upper left*: Histogram of V_ϕ for stars with revised C10 distances, with spectroscopically assigned D classifications, [Fe/H] < -2.0, and $Z_{\rm max} > 5$ kpc. The red solid lines are the suggested components from the R-Mix procedure, while the blue solid line is the final mixture model. *Upper right*: Similar, for D stars with I08 distances. *Lower left*: Similar, for D stars with A11 distances. *Lower right*: Similar, for D stars with S10 distances.

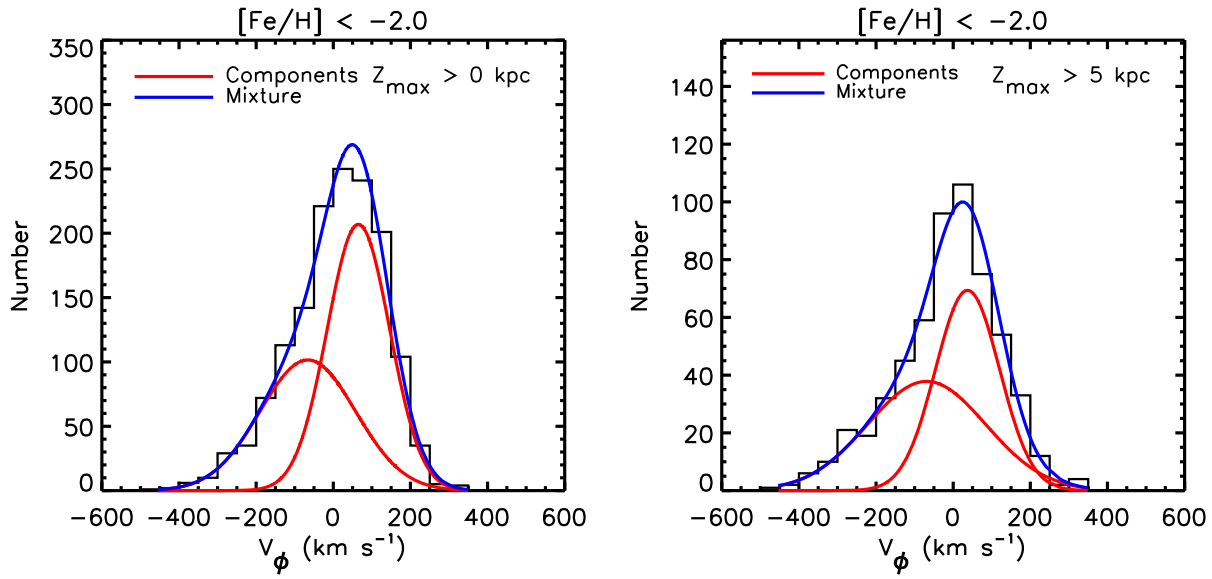

Fig. 11.— *Left panel*: Histogram of V_ϕ for stars with revised C10 distances, with spectroscopically assigned D, TO, and SG/G classifications, [Fe/H] < -2.0, and all values of $Z_{\rm max}$. The red solid lines are the suggested components from the R-Mix procedure, while the blue solid line is the final mixture model. *Right Panel*: Similar, but for stars with $Z_{\rm max} > 5$ kpc.

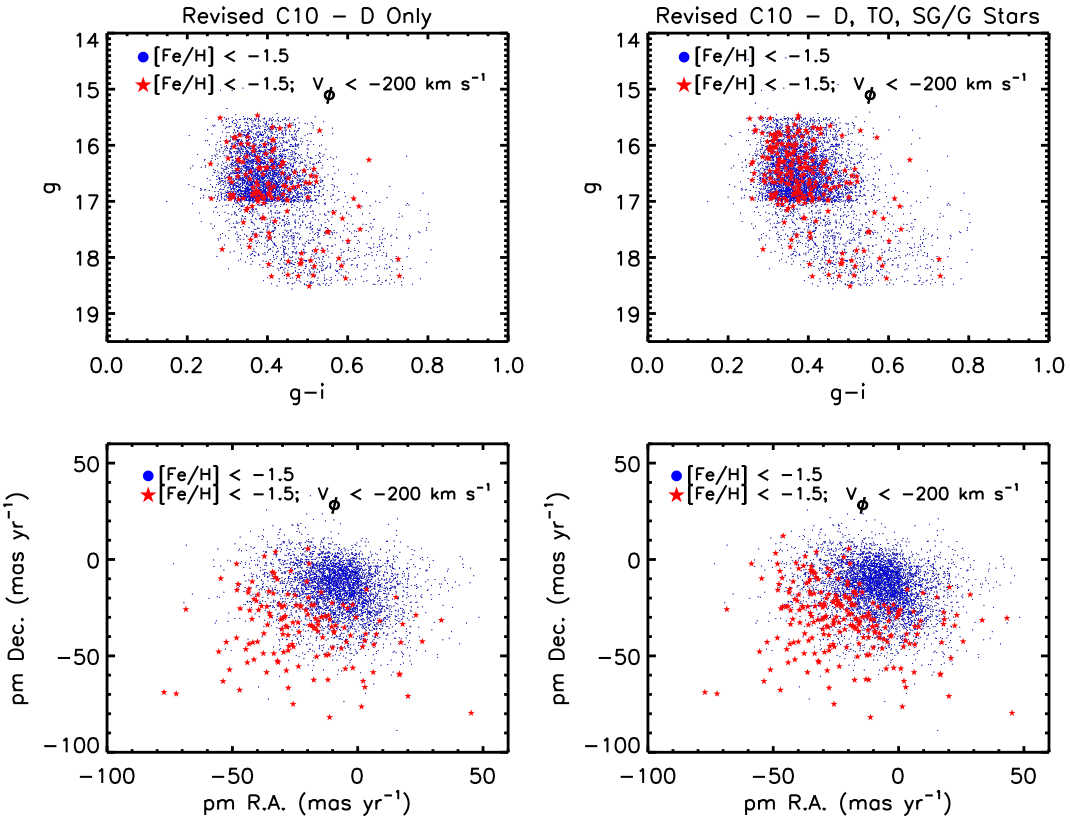

Fig. 12.— *Upper left*: Apparent g-band magnitude vs. $g-i$ colors for the C10 stars with revised distances and [Fe/H] < -1.5, exclusively for stars spectroscopically classified as D. The stars with highly-retrograde motions, $V_\phi < -200$ km s^{-1}, are indicated by the red stars; the rest of the sample is indicated with blue dots. The apparent structure as a function of g magnitude in this diagram is due to the different selections used for the two classes of calibration stars. *Upper right*: Similar, but for the full set of C10 classifications, D, TO, and SG/G. *Lower left*: The proper motion distribution (vector components along the R.A. and Dec. directions) for the C10 stars with revised distances and [Fe/H] < -1.5, exclusively for stars spectroscopically classified as D. The stars with highly-retrograde motions, $V_\phi < -200$ km s^{-1}, are indicated by the red stars; the rest of the sample is indicated with blue dots. *Lower right*: Similar, but for the full set of C10 classifications, D, TO, and SG/G.

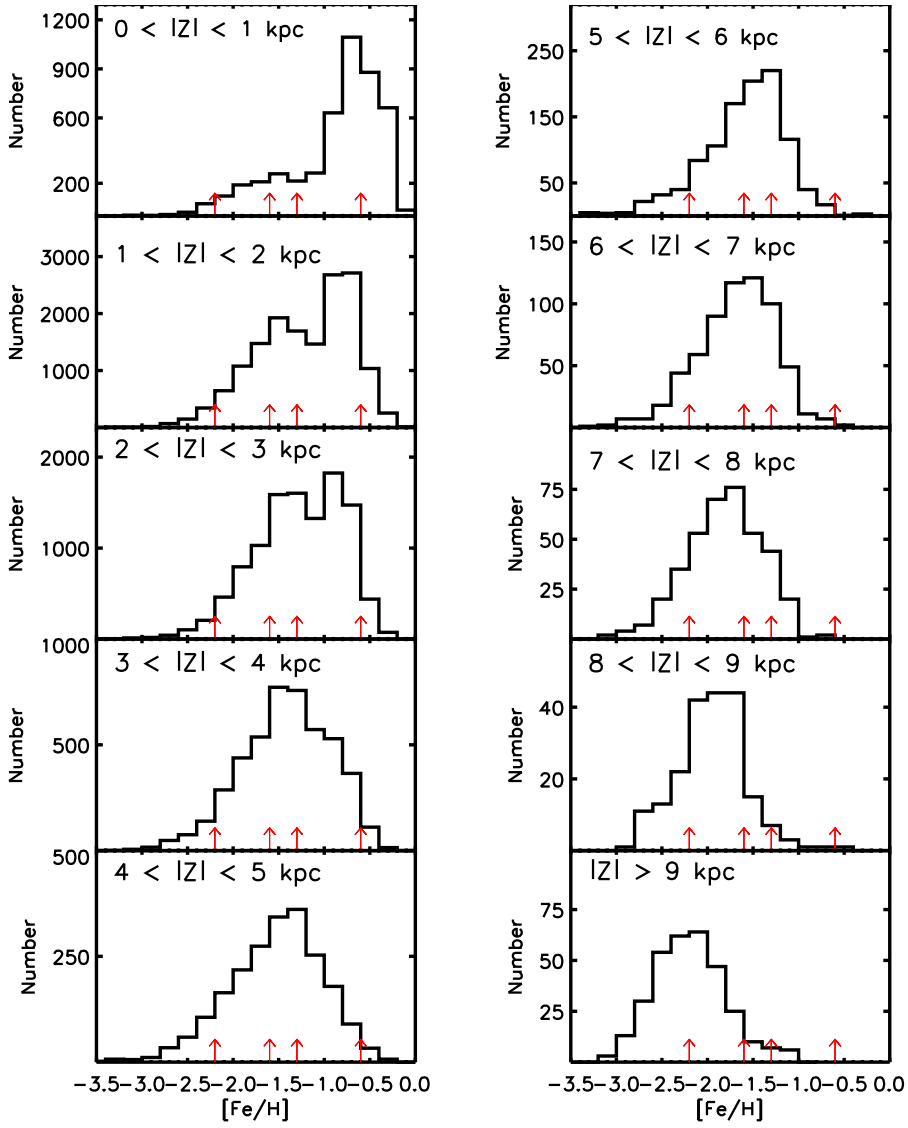

Fig. 13.— As-observed metallicity distribution functions for stars from C10 with revised distances, for various cuts in distance from the Galactic plane, $|Z|$. The vertical red arrows mark the positions of the primary stellar components modeled by C10, the thick disk ([Fe/H] = −0.6), the metal-weak thick disk ([Fe/H] = −1.3), the inner halo ([Fe/H] = −1.6), and the outer halo ([Fe/H] = −2.2).

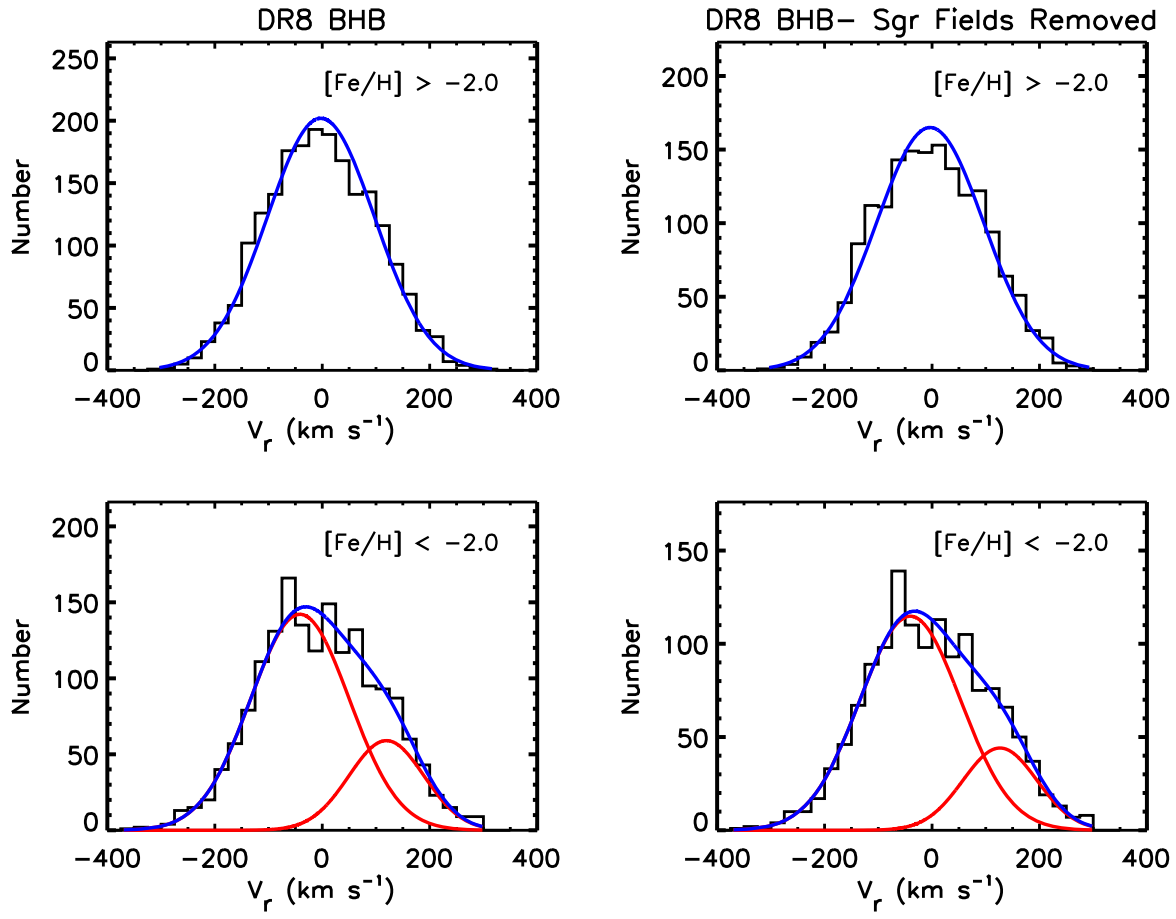

Fig. 14.— *Left Panels:* Distribution of Galactocentric radial velocities for a sample of well-classified Blue Horizontal-Branch (BHB) stars, based on the sample from SDSS DR8 of Xue et al. (2011), including stars in the range of Galactocentric distance $5 < r < 40$ kpc, and with $|Z| > 4$ kpc. In the top panel, the blue line is the best-fit Gaussian for stars with [Fe/H] > -2.0. In the bottom panel, for stars with [Fe/H] < -2.0, the red lines represent components of the best two-component fit suggested by R-Mix, and the blue line is the resulting mixture model. *Right Panels:* Similar, but for the case where BHB stars from plug-plates in the direction of the two most prominent wraps of the Sagittarius tidal stream have been removed. The metallicity estimates are based on those derived using the procedures described by Wilhelm, Beers, & Gray (1999), which are optimal for these warmer stars ($T_{\rm eff} > 7000$ K).

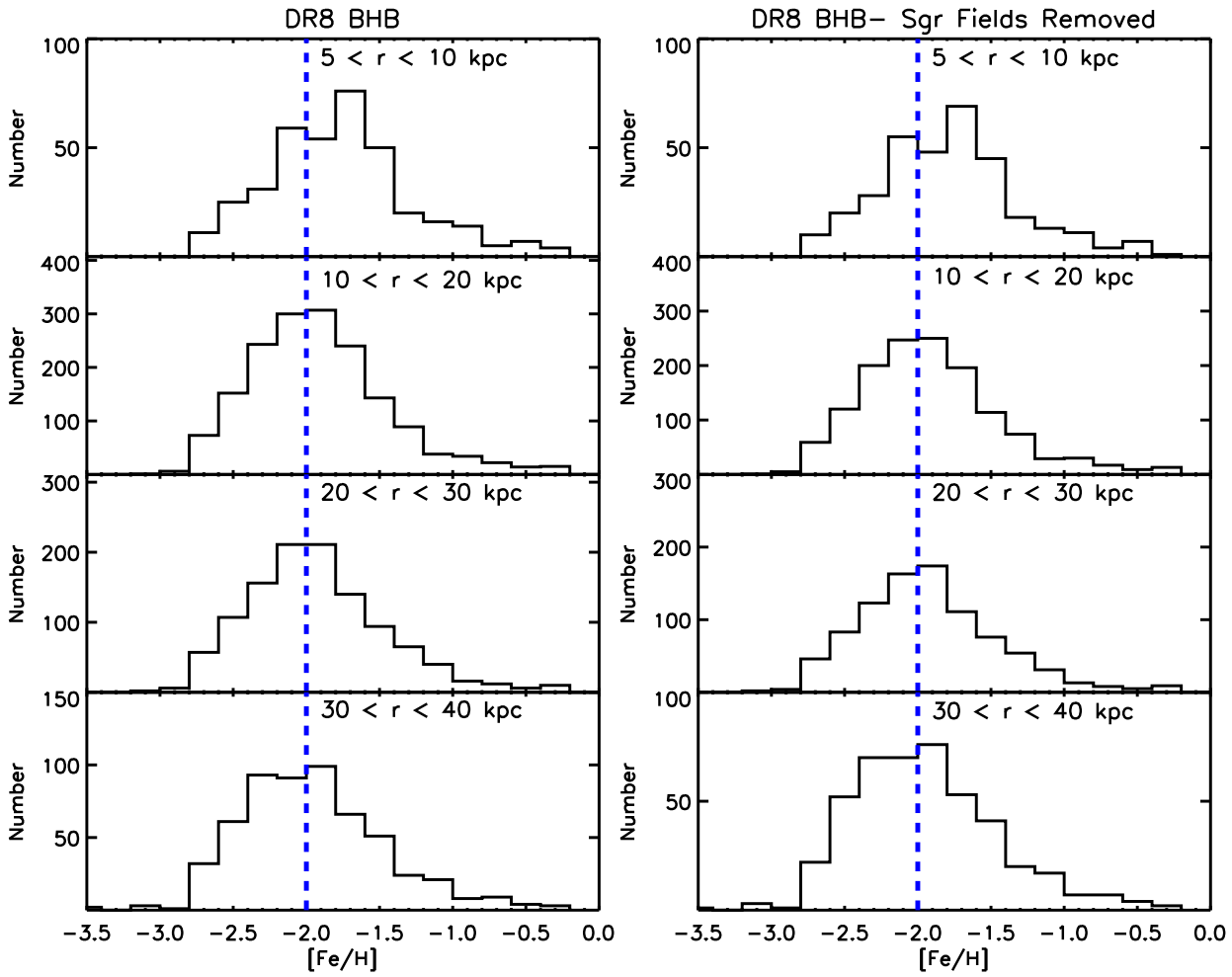

Fig. 15.— *Left Panels:* As-observed MDF for the Xue et al. (2011) BHB stars for various cuts on the distance from the Galactic center, r. Stars with $|Z|< 4$ kpc have been removed from the sample. *Right Panels:* Similar, but for the case where BHB stars from plug-plates in the direction of the two most prominent wraps of the Sagittarius tidal stream have been removed. In both cases, the nature of the MDF appears to shift from the top panels, which exhibit distributions that we associate with the inner-halo population, over to distributions in the lower three panels that are dominated by the outer-halo population. The metallicity estimates are based on those derived using the procedures described by Wilhelm, Beers, & Gray (1999), which are optimal for these warmer stars ($T_{\rm eff} > 7000$ K). The dashed blue line provides a reference at [Fe/H]$= -2.0$.